UC Davis
UC Davis Previously Published Works

Title
Excessive laughter-like vocalizations, microcephaly, and translational outcomes in the Ube3a deletion rat model of Angelman Syndrome

Permalink
https://escholarship.org/uc/item/8fz2b3z9

Journal
Journal of Neuroscience, 41(42)

ISSN
0270-6474

Authors
Berg, Elizabeth L
Jami, Shekib A
Petkova, Stela P
et al.

Publication Date
2021-10-20

DOI
10.1523/jneurosci.0925-21.2021

Peer reviewed

eScholarship.org Powered by the California Digital Library
University of California

JNeurosci Accepted Manuscript

JNeurosci
THE JOURNAL OF NEUROSCIENCE

Research Articles: Behavioral/Cognitive

Excessive laughter-like vocalizations, microcephaly, and translational outcomes in the *Ube3a* deletion rat model of Angelman Syndrome

https://doi.org/10.1523/JNEUROSCI.0925-21.2021

Cite as: J. Neurosci 2021; 10.1523/JNEUROSCI.0925-21.2021

Received: 29 April 2021
Revised: 23 August 2021
Accepted: 26 August 2021

This Early Release article has been peer-reviewed and accepted, but has not been through the composition and copyediting processes. The final version may differ slightly in style or formatting and will contain links to any extended data.

Alerts: Sign up at www.jneurosci.org/alerts to receive customized email alerts when the fully formatted version of this article is published.

Copyright © 2021 Berg et al.
This is an open-access article distributed under the terms of the Creative Commons Attribution 4.0 International license, which permits unrestricted use, distribution and reproduction in any medium provided that the original work is properly attributed.

JNeurosci Accepted Manuscript

1 **Excessive laughter-like vocalizations, microcephaly, and translational outcomes in the**
2 ***Ube3a* deletion rat model of Angelman Syndrome**
3

4 Elizabeth L. Berg[1], Shekib A. Jami[2], Stela P. Petkova[1], Annuska Berz[3,4], Timothy A. Fenton[1], Jason P.
5 Lerch[5,6,7], David J. Segal[8], John A. Gray[2], Jacob Ellegood[5], Markus Wöhr[3,4,9,10], and Jill L. Silverman[1]*
6
7 [1]MIND Institute and Department of Psychiatry and Behavioral Sciences, University of California Davis
8 School of Medicine, Sacramento, CA 95817, USA. [2]Department of Neurology, Center for Neuroscience,
9 University of California Davis, Davis, CA 95618, USA. [3]Behavioral Neuroscience, Experimental and
10 Biological Psychology, Faculty of Psychology, Philipps-University Marburg, 35032 Marburg, Germany.
11 [4]Center for Mind, Brain and Behavior, Philipps-University Marburg, 35032 Marburg, Germany. [5]Mouse
12 Imaging Centre, The Hospital for Sick Children, Toronto, ON M5T 3H7, Canada. [6]Department of
13 Medical Biophysics, University of Toronto, Toronto, ON M5S, Canada. [7]Wellcome Centre for Integrative
14 Neuroimaging, The University of Oxford, Oxford OX3 9DU, UK. [8]MIND Institute, Genome Center, and
15 Department of Biochemistry and Molecular Medicine, University of California Davis, Davis, CA 95616,
16 USA. [9]KU Leuven, Faculty of Psychology and Educational Sciences, Research Unit Brain and Cognition,
17 Laboratory of Biological Psychology, Social and Affective Neuroscience Research Group, B-3000
18 Leuven, Belgium. [10]KU Leuven, Leuven Brain Institute, B-3000 Leuven, Belgium.
19
20 ***Corresponding Author:**
21 Jill L. Silverman
22 MIND Institute and Department of Psychiatry and Behavioral Sciences
23 University of California Davis School of Medicine
24 Research II Building 96, 4625 2nd Avenue, Suite 1001B
25 Sacramento, CA 95817
26 Phone: 916-734-8531
27 jsilverman@ucdavis.edu
28
29 **Running title:** USV and AS-relevant outcomes in the *Ube3a* rat
30

31 **Keywords:** Ube3a, Angelman Syndrome, rat model, behavior, ultrasonic vocalizations, play, gait,
32 learning, memory, long term potentiation, MRI.
33
34 **Number of pages:** 38
35 **Number of figures:** 6
36 **Number of extended data figures:** 2
37 **Number of words in abstract:** 162
38 **Number of words in introduction:** 589
39 **Number of words in discussion:** 1500
40
41 **Conflict of Interest:** The authors declare no conflicts of interest.
42
43 **Acknowledgments:** This work was supported by the Foundation for Angelman Syndrome Therapeutics
44 (FAST; ELB, DJS, JLS), the MIND Institute's Intellectual and Developmental Disabilities Resource
45 Center NIH U54HD079125 (JLS; PI LA), the NIMH R01MH117130 (JAG), the Deutsche
46 Forschungsgemeinschaft (DFG WO 1732/4-2; MW), the Canadian Institute for Health Research (CIHR;
47 JPL, JE), the Ontario Brain Institute (OBI; JPL, JE), and the Gustav Adolf Lienert Foundation (AB). The
48 authors thank Matthew Matson, Ruona Lin, Steven Xiong, Yutian Shen, and Anurupa Kar for technical
49 support.

JNeurosci Accepted Manuscript

50 **Abstract**

51

52 Angelman Syndrome (AS) is a rare genetic neurodevelopmental disorder characterized by
53 intellectual disabilities, motor and balance deficits, impaired communication, and a happy, excitable
54 demeanor with frequent laughter. We sought to elucidate a preclinical outcome measure in male and
55 female rats that addressed communication abnormalities of AS and other neurodevelopmental disorders in
56 which communication is atypical and/or lack of speech is a core feature. We discovered, and herein report
57 for the first time, excessive laughter-like 50-kHz ultrasonic emissions in the *Ube3a*$^{mat-/pat+}$ rat model of
58 AS, which suggests an excitable, playful demeanor and elevated positive affect, similar to the demeanor
59 of individuals with AS. Also in line with the AS phenotype, *Ube3a*$^{mat-/pat+}$ rats demonstrated aberrant
60 social interactions with a novel partner, distinctive gait abnormalities, impaired cognition, an underlying
61 long-term potentiation deficit, and profound reductions in brain volume. These unique, robust phenotypes
62 provide advantages compared to currently available mouse models and will be highly valuable as
63 outcome measures in the evaluation of therapies for AS.

64

65 **Significance Statement**

66

67 Angelman Syndrome (AS) is a severe neurogenetic disorder for which there is no cure, despite
68 decades of research using mouse models. This study utilized a recently developed rat model of AS to
69 delineate disease-relevant outcome measures in order to facilitate therapeutic development. We found the
70 rat to be a strong model of AS, offering several advantages over mouse models by exhibiting numerous
71 AS-relevant phenotypes including overabundant laughter-like vocalizations, reduced hippocampal long-
72 term potentiation, and volumetric anomalies across the brain. These findings are unconfounded by
73 detrimental motor abilities and background strain, issues plaguing mouse models. This rat model
74 represents an important advancement in the field of AS and the outcome metrics reported herein will be
75 central to the therapeutic pipeline.

JNeurosci Accepted Manuscript

76

77 **Introduction**

78

79 Angelman Syndrome (AS) is a rare neurodevelopmental disorder (NDD) characterized by
80 intellectual disability, impaired communication, ataxia, seizures, as well as a happy disposition with a
81 high degree of excitability, smiling, and easily provoked laughter (Williams and Franco, 2010). AS is
82 caused by dysfunction of maternal ubiquitin protein ligase E3A (UBE3A), typically from a de novo
83 deletion in the 15q11-q13 region (Albrecht et al., 1997). Restoring functional UBE3A is seemingly
84 possible by innovative gene therapy approaches including antisense oligonucleotides (Meng et al., 2015),
85 viral vector delivery (Daily et al., 2011), artificial transcription factors (Bailus et al., 2016), stem cell
86 mediated therapies (Adhikari et al., 2021), and the cutting edge Cas9 (Wolter et al., 2020). Gene
87 replacement therapy is therefore on the horizon for AS and, indeed, two clinical trials using "gene
88 therapy-like" antisense oligonucleotide interventions began recruitment in 2020 (GeneTx NCT04259281;
89 Roche NCT04428281).
90 Indispensable to such a strategy of therapeutic development are *in vivo* studies utilizing
91 preclinical model systems with rigorous translational outcomes. One domain that is critically impaired in
92 AS and other NDDs but difficult to study in preclinical models due to their lack of human-interpretable
93 language is communication. The increasing availability of rat models of NDDs opens up new
94 opportunities to develop preclinical outcome measures of social communication. While the mouse has
95 been the preferred model species in recent decades due to the genetic technologies available, there are
96 complex behaviors and physiological processes difficult or impossible to investigate in mice that are
97 easily observable in rats (Ellenbroek and Youn, 2016; Hofer et al., 2002; Portfors, 2007; Hammerschmidt
98 et al., 2012; Wöhr and Schwarting, 2013; Portfors and Perkel, 2014).
99 One prominent example is the greater sophistication and complexity in the rat acoustic
100 communication system. While both mice and rats emit ultrasonic vocalizations (USV), rats emit USV that
101 serve as situation-dependent, evolved signals which accomplish important communicative functions that

JNeurosci Accepted Manuscript

are not observed as functions of mouse USV, such as low-frequency 22-kHz “alarm calls” which rats use to warn of potential threats (Brudzynski, 2013; Wöhr and Schwarting, 2013; Blanchard et al., 1991; Sadananda et al., 2008; Fendt et al., 2018; Wöhr and Schwarting, 2007; Kisko et al., 2017). The recent generation of the first rat model of AS therefore provides the unique opportunity to utilize a greater diversity of social and communication behaviors as compared to those previously available in mouse models (Jiang et al., 2010; Huang et al., 2013; Dutta and Crawley, 2020; Kondrakiewicz et al., 2019; Netser et al., 2020; Parker et al., 2014; Ellenbroek and Youn, 2016; Homberg et al., 2017; Reppucci et al., 2020).

To build upon the initial reports describing the *Ube3a* deletion rat model of AS, which revealed deficits in motor, cognition, social approach, and pup vocalizations (Berg et al., 2020c; Dodge et al., 2020), we sought to investigate nuanced social behaviors and further characterize vocalization patterns. With numerous novel therapies being assessed in clinical trials and at the investigational drug discovery level, AS-relevant outcome measures are vital for demonstrating functional efficacy of the varied intervention approaches. Leveraging the rat’s social communication system, we discovered that the *Ube3a* maternal deletion rat (*Ube3a*$^{mat-/pat+}$) produces excessive signals of positive affect characteristic of AS. Several other AS-relevant phenotypes were evident, including atypical social interactions and maladaptive impairments in gait and cognition. We also identified reduced hippocampal long-term potentiation, observed in mouse models of AS but not yet in rats, as a putative cellular mechanism underlying the learning and memory deficits apparent in the model. Finally, our neuroimaging analysis revealed decreased brain volume and pronounced increasing severity with age.

Materials and Methods

Subjects. Subjects were male and female Sprague Dawley *Ube3a*$^{mat-/pat+}$ rats and their wildtype littermates (*Ube3a*$^{mat+/pat+}$) generated from breeding pairs of paternal *Ube3a* deletion females and wildtype males purchased from Envigo (Indianapolis, IN). The initial generation of *Ube3a* deletion rats using

JNeurosci Accepted Manuscript

128 CRISPR/Cas9 was described previously (Berg et al., 2020c). Genotyping was performed using a small
129 sample of tail tissue collected at postnatal day (PND) 2, REDExtract-N-Amp (Sigma Aldrich, St. Louis,
130 MO, USA), and primers Rube1123 TAGTGCTGAGGCACTGGTTCAGAGC, Rube1606r
131 TGCAAGGGGTAGCTTACTCATAGC, Ub3aDelSpcfcF6 ACCTAGCCCAAAGCCATCTC, and
132 Ub3aDelR2 GGGAACAGCAAAAGACATGG. All animals were socially housed in a temperature-
133 controlled vivarium maintained on a 12:12 light-dark cycle with testing occurring during the light
134 phase. All procedures were conducted in compliance with the NIH Guidelines for the Care and Use of
135 Laboratory Animals and approved by the Institutional Animal Care and Use Committee of the University
136 of California Davis. To minimize the carry-over effects from repeated testing and handling, seven mixed-
137 sex cohorts of rats were tested and behavioral tests were carried out in order of least to most stressful with
138 at least 48 hrs break between tests. Each cohort was comprised of four to nine litters and subjects were
139 sampled as followed: subjects for 50-kHz ultrasonic (USV) playback were sampled from Cohort 1;
140 contextual and cued fear conditioning from Cohort 2; gait analysis, heterospecific play, and social play
141 from Cohort 3; acoustic startle and long-term potentiation from Cohort 4; spontaneous exploratory USV
142 from Cohort 5; spontaneous alternation from Cohort 6; and olfactory discrimination from Cohort 7.
143 Following behavioral testing, rats from Cohort 3 were perfused for magnetic resonance imaging.
144
145 **Juvenile USV in response to heterospecific play.** At postnatal day (PND) 30 through 34, rats
146 were provided daily heterospecific play sessions involving manual stimulation using a slightly
147 abbreviated procedure from those described previously (Burgdorf and Panksepp, 2001; Schwarting et al.,
148 2007; Wöhr et al., 2009). For 5 min on 5 consecutive days, rats were individually manipulated by a
149 familiar experimenter using a single clean hand within a clean, empty version of the home cage with fresh
150 bedding (37.2 cm l x 30.8 cm w x 18.7 cm h; illuminated to ~30 lux) while vocalizations were recorded
151 with an overhead ultrasonic microphone (Avisoft Bioacoustics, Glienicke, Germany) for later scoring by
152 a trained observer blinded to genotype. The number of calls emitted during each 30-sec interval were
153 counted and classified as either high (50-kHz) or low (short 22-kHz) frequency using a threshold of 33

JNeurosci Accepted Manuscript

154 kHz. Calls emitted during the minute immediately preceding the heterospecific play sessions on days 2-4
155 ("anticipation") were also counted and classified.
156 All rats were handled by the experimenter in a standardized fashion (5 min on 3 days) prior to the
157 first heterospecific play session. The physical manipulations performed were tickling the subject's neck
158 (2x), tickling the subject's belly (1x), pushing into their shoulders ("push and drill"; 1x), and flipping the
159 subject onto their back and momentarily pinning them down ("flip over"; 3x). Each manipulation lasted
160 30 sec with three 30-sec breaks interspersed at 0, 60, and 150 sec, during which the experimenter did not
161 initiate touching the subject but moved their hand around the cage to encourage following or chasing. In
162 an effort to provide a standardized experience, a single experimenter carried out the procedure for all
163 subjects and the experimenter remained unaware of USV being emitted during the test, performing the
164 manipulations in an equivalent manner for all rats. To mitigate any potential effect of order, the sequence
165 of manipulations was re-ordered each day but remained consistent across all animals. The testing order of
166 the subjects was also changed from day to day.
167
168 **Juvenile spontaneous exploratory USV.** At PND 30, rats were individually placed in a clean,
169 empty version of the home cage (illuminated to ~30 lux) with clean bedding for 5 min similarly to
170 methods described previously (Schwarting et al., 2007; Wöhr et al., 2008). Recording of ultrasonic
171 vocalizations began immediately following the subject being placed into the cage and no other animals or
172 any experimenter were present in the room during recording. Calls were classified by a trained observer
173 blinded to genotype as either high (50-kHz) or low (short 22-kHz) frequency using a threshold of 33 kHz.
174
175 **Juvenile USV in response to playback of 50-kHz USV.** At PND 30±4, subjects were
176 individually presented with 1-min of natural pro-social 50-kHz USV while on a radial maze illuminated
177 to ~8 lux as described previously (Berg et al., 2018; Berg et al., 2020c). USV were presented to individual
178 subjects using an established playback paradigm (Berg et al., 2018; Wöhr et al., 2016), including the USV
179 stimulus previously demonstrated to elicit social approach (behavior shown in Berg et al., 2020c). The

JNeurosci Accepted Manuscript

180 USV stimulus consisted of 221 natural 50-kHz USV recorded from a naïve male rat during exploration of
181 a cage containing a recently separated cage mate. A 3.5-sec sequence of 13 calls was repeated 17 times
182 such that 221 50-kHz calls were presented within 1 min. Response vocalizations were recorded with an
183 overhead ultrasonic microphone (Avisoft Bioacoustics) and the number of calls emitted during the minute
184 of playback were counted by a trained observer blinded to genotype and classified as high (50-kHz)
185 or low (short 22-kHz) frequency using a threshold of 33 kHz.
186
187 **Juvenile social play.** At PND 38±1, social play behavior was assessed following a protocol
188 described previously (Berg et al., 2018; Berg et al., 2020a; Berg et al., 2020b). Each subject rat was
189 placed with a freely moving, unfamiliar, strain-, sex-, and age-matched wildtype stimulus rat for 10 min
190 in a clean, empty test arena (illuminated to ~30 lux) containing a thin layer of clean bedding. In order to
191 facilitate social play, each subject and stimulus animal was socially isolated in a separate holding room
192 for 30 min prior to the test. Stimulus animals were generated from wildtype Sprague-Dawley breeders
193 (Envigo, Indianapolis, IN) and handled in a standardized manner (5 min on 3 days) prior to the assay. The
194 interaction was video-recorded, and behaviors were later scored by a trained observer blinded to genotype
195 as follows: Social sniffing: sniffing the stimulus rat's face, body, or tail; Anogenital sniffing: sniffing the
196 stimulus rat's anogenital region; Self-grooming: subject grooming itself; Exploring: sitting, walking,
197 rearing, or sniffing the ground or wall; Following or chasing: following (walking pace) or chasing
198 (running pace) the stimulus rat; Rough-and-tumble playing: accelerated movement involving chasing,
199 pouncing, pinning, tumbling, and/or boxing which requires the stimulus rat's participation (i.e.,
200 reciprocity); Push past: directed movement toward the stimulus rat to get next to, or move closely past,
201 without sniffing or otherwise engaging; Push under or crawl over: head dip under the stimulus rat's belly
202 or completely stepping over the stimulus rat; Pounce: both paws placed via leap or directed movement
203 onto the stimulus rat's back. Blind scoring was possible since *Ube3a*$^{mat-/pat+}$ rats have normal body weight
204 and are physically indistinguishable from their wildtype littermates (Berg et al., 2020c).
205

JNeurosci Accepted Manuscript

206 **Olfactory discrimination.** At 42±3, the ability of rats to discriminate between a social and non-
207 social odor was tested by measuring the time spent investigating odor-saturated cotton swabs. Subjects
208 were individually tested in clean chambers (40.6 cm l x 40.6 cm w x 28 cm h) dimly illuminated to ~30
209 lux. On the day before the test, rats were habituated to the test chamber containing a clean dry cotton
210 swab (15.2 cm l) for 20 min. The tip of the swab was secured 3 cm above the floor in the center of the
211 arena by being attached to the top of a clean weighted glass dome (7.6 cm d x 10 cm h) and angled
212 downward. On the day of the test, rats were again habituated to the arena containing a clean dry cotton
213 swab for 10 min, followed by a swab soaked in water, then vanilla (1:100 dilution; McCormick, Hunt
214 Valley, MD), and then a social scent. The social scent was collected by wiping a cotton swab in a zig zag
215 pattern along the bottom of a cage of same sex but unfamiliar Sprague Dawley rats (Envigo, Indianapolis,
216 IN). Each saturated swab was presented for 2 min and the order of odor presentation was consistent across
217 all animals. Time spent sniffing the swab soaked with vanilla scent and the swab soaked with social scent
218 (defined as the nose within 2 cm of the cotton swab tip) was measured using videotracking software
219 (EthoVision XT, Noldus Information Technology, Leesburg, VA), which was subsequently validated
220 manually.
221
222 **Juvenile gait.** At PND 25, gait metrics were collected using the DigiGait automated treadmill
223 system and analysis software (Mouse Specifics, Inc., Framingham, MA). Subjects were placed
224 individually into the enclosed treadmill chamber and allowed to acclimate before the belt was turned on.
225 The belt speed was slowly increased to a constant speed of 20 cm/sec, at which each rat was recorded
226 making clearly visible consecutive strides for 3-6 sec.
227
228 **Juvenile contextual and cued fear conditioning.** At PND 43±1, learning and memory were
229 assessed using an automated fear conditioning chamber (Med Associates, Inc., Fairfax, VT) following
230 methods previously described (Copping et al., 2017; Adhikari et al., 2018; Berg et al., 2020b). On day
231 one, rats were trained via exposure to a series of three noise-shock (conditioned stimulus-unconditioned

JNeurosci Accepted Manuscript

232 stimulus; CS-US; 80 dB white noise, 0.7 mA foot shock) pairings inside a sound-attenuated chamber
233 with specific visual, tactile, and odor cues. On day two, contextual memory was tested by placing each
234 subject back inside the training environment (no noise or foot shock occurred). On day three, cued
235 memory was evaluated by placing subjects into a novel context with altered visual, tactile, and odor cues.
236 Following a period of exploration, the white noise CS was presented for 3 min. Time spent freezing was
237 measured using VideoFreeze software (Med Associates, Inc.).
238
239 **Prepulse inhibition of an acoustic startle response.** At 9-10 weeks of age, prepulse inhibition
240 was measured using an SR-Lab System (San Diego Instruments, San Diego, CA). Subjects were placed in
241 a clear plastic cylinder, which was mounted onto a platform connected to piezoelectric transducers inside
242 a sound-attenuating chamber with internal speakers. The background noise level in the chamber was 70
243 decibel (dB) white noise. Each session consisted of a 5-min acclimation period followed by a pseudo-
244 randomized presentation of 50 trials of five different trial types: one trial type was a 40-ms 120-dB startle
245 stimulus, three trial types involved an acoustic prepulse (74, 82, or 90 dB) presented 120 ms prior to the
246 120-dB startle stimulus, and there were also trials with no startle stimulus in order to measure baseline
247 movement inside the cylinder. Each trial type was presented in 10 blocks and was randomized within
248 blocks. The intertrial interval varied randomly between 10 sec and 20 sec. Percent PPI was calculated
249 using the equation: % PPI = [1 – (Prepulse/Max Startle)] x 100.
250
251 **Spontaneous alternation.** At 10 weeks of age, spontaneous alternation was measured by
252 allowing rats to freely explore a novel Y-maze (black, opaque; arms: 21” l x 4.5” w x 11” h; illuminated
253 to ~30 lux) for 8 min. An overhead camera connected to videotracking software (EthoVision XT; Noldus
254 Information Technology, Wageningen, Netherlands) was used to quantify the number of arm entries, the
255 number of errors (defined as the sum of direct and indirect revisits to an arm), the number of spontaneous
256 alternations, and the maximum number of possible alternations for the entire session.
257

JNeurosci Accepted Manuscript

258 **Long-term potentiation (LTP).** *Acute slice preparation.* At 12-13 weeks of age, subjects were
259 deeply anesthetized with isoflurane and, following decapitation, the brain was rapidly removed and
260 submerged in ice-cold, oxygenated (95% O_2/5% CO_2) ACSF containing (in mM) as follows: 124 NaCl, 4
261 KCl, 25 $NaHCO_3$, 1 NaH_2PO_4, 2 $CaCl_2$, 1.2 $MgSO_4$, and 10 glucose. On an ice-cold plate, the brain
262 hemispheres were separated, blocked, and the hippocampi removed. The 400-μmat-thick slices were then
263 cut using a McIlwain tissue chopper (Brinkman, Westbury, NY). Slices from the dorsal thirds of the
264 hippocampus were used. Slices were incubated (at 33°C) for 20 min and then maintained in submerged-
265 type chambers that were continuously perfused (2-3 mL/min) with ACSF and allowed to recover for at
266 least 1.5-2 hr before recordings. Just prior to start of experiments slices were transferred to a submersion
267 chamber on an upright Olympus microscope, perfused with 30.4°C normal ACSF saturated with 95%
268 O_2/5% CO_2.

269 *Electrophysiological recordings.* A bipolar, nichrome wire stimulating electrode (MicroProbes)
270 was placed in stratum radiatum of the CA1 region and used to activate Schaffer collateral/commissural
271 fiber synapses. Evoked fEPSPs (basal stimulation rate = 0.033 Hz) were recorded in *stratum radiatum*
272 using borosilicate pipettes (Sutter Instruments, Novato, CA) filled with ACSF (resistance 5-10 mΩ).
273 Submerged-type recording chambers were used for all recordings. All recordings were obtained with a
274 MultiClamp 700B amplifier (Molecular Devices, San Jose, CA), filtered at 2 kHz, digitized at 10 Hz. To
275 determine response parameters of excitatory synapses, basal synaptic strength was determined by
276 comparing the amplitudes of presynaptic fiber volleys and postsynaptic fEPSP slopes for responses
277 elicited by different intensities of SC fiber stimulation. Presynaptic neurotransmitter release probability
278 was compared by paired pulse facilitation (PPF) experiments, performed at 25, 50, 100 and 250 msec
279 stimulation intervals. LTP was induced by high frequency stimulation (HFS) using a 2x tetanus (1-s-long
280 train of 100 Hz stimulation) with a 10 sec inter-tetanus interval. At the start of each experiment, the
281 maximal fEPSP amplitude was determined and the intensity of presynaptic fiber stimulation was adjusted
282 to evoke fEPSPs with an amplitude ~40-50% of the maximal amplitude. The average slope of EPSPs
283 elicited 55-60 min after HFS (normalized to baseline) was used for statistical comparisons.

JNeurosci Accepted Manuscript

284

285 **Magnetic resonance imaging (MRI).** At 6.5 months of age, *ex vivo* neuroimaging was carried
286 out by following a protocol previously described (Berg et al., 2018; Berg et al., 2020c). Brains were
287 flushed and fixed via transcardial perfusion with 50 mL phosphate-buffered saline (PBS) containing 10
288 U/mL heparin and 2 mM ProHance (gadolinium contrast agent; Bracco Diagnostics Inc., Monroe
289 Township, NJ) followed by 50 mL 4% paraformaldehyde in PBS containing 2 mM ProHance. Brains
290 were incubated in the 4% PFA solution at 4°C for 24 hrs, transferred to a 0.02% sodium azide PBS
291 solution, and then incubated at 4°C for at least one month before being scanned. Magnetic resonance
292 imaging (MRI) of the brains within their skulls was carried out using a multi-channel 7.0 Tesla scanner
293 (Agilent Inc., Palo Alto, CA). Seven custom millipede coils were used to image the brains in parallel
294 (Bock et al., 2005; Lerch et al., 2011). Parameters used in the anatomical MRI scans: T2 weighted 3D fast
295 spin echo sequence, with a cylindrical acquisition of k-space, and with a TR of 350 ms, and TEs of 10.5
296 ms per echo for 12 echoes, field of view 36 x 36 x 40 mm^3 and a matrix size of 456 x 456 x 504 giving an
297 image with 0.079 mm isotropic voxels (Noakes et al., 2017). The current scan time for this sequence is ~
298 3 hours.

299 To visualize and compare any changes in the rat brains the images were linearly and non-linearly
300 registered together using the pydpiper framework. Registrations were performed using a combination of
301 mni_autoreg tools (Collins et al., 1994) and ANTS (advanced normalization tools) (Avants et al., 2011).
302 Following registration, a population atlas was created representing the average anatomy of the study
303 sample. At the end of the registration process all the scans were deformed into alignment with one another
304 in an unbiased fashion. This allows for analysis of the deformations required to register the brains
305 together, which can be used to assess the volume of the individual brains and compared them to one
306 another (Bishop et al., 2006; Lerch et al., 2008c; Lerch et al., 2008a; Lerch et al., 2008b; Nieman et al.,
307 2010; Nieman et al., 2018). For comparisons to the juvenile brains, a separate registration pipeline was
308 used that included all the brains from this study as well as the previous Berg et al. (2020) study.
309 Volumetric differences were calculated on a regional and a voxelwise basis. An in-house manually

JNeurosci Accepted Manuscript

310 segmented hierarchical rat brain atlas was used to calculate the volumes of 52 different segmented
311 structures. These structures were derived from multiple atlases (Dorr et al., 2008; Steadman et al., 2014)
312 and then modified for use in the rat brain.
313
314 **Experimental design and statistical analyses.** Statistical analyses were performed using
315 GraphPad Prism 8 statistical software (GraphPad Software, San Diego, CA). Clampex 10.6 software suite
316 (Molecular Devices, San Jose, CA) was used for analyzing electrophysiological data. Congruent with
317 previous studies, no significant sex differences were detected so the results herein include both males and
318 females. Effect sizes and power were determined using Cohen's *d*.
319 *Analysis of behavior and LTP.* For single comparisons between two groups, either a Student's *t*-
320 test or Mann-Whitney *U* test was used. Data that passed distribution normality tests, were collected using
321 continuous variables, and had similar variances across groups were analyzed via Student's *t*-test.
322 Alternatively, a Mann-Whitney *U* test was used. Either a two-way analysis of variance (ANOVA) or two-
323 way repeated measures ANOVA was used to analyze the effects of genotype and a second factor. In
324 repeated measures ANOVA, genotype was the between-group factor and time, limb set, test phase, scent,
325 or prepulse intensity was the within-group factor. *Post-hoc* comparisons were performed following a
326 significant main effect or interaction and were carried out using Holm-Sidak's multiple comparisons test
327 controlling for multiple comparisons. Data points within two standard deviations of the mean were
328 included, all significance tests were two-tailed, and a p-value of < 0.05 was considered significant.
329 *Analysis of MRI.* Statistical analyses were used to compare both the absolute and relative volumes
330 voxelwise as well as across the 52 different hierarchical structures in the rat brains. Absolute volume was
331 calculated as mm^3 and relative volume was assessed as a measure of % total brain volume. Voxelwise and
332 regional differences were assessed using linear models. All image analysis tools and software is available
333 on Github (https://github.com/Mouse-Imaging-Centre). Multiple comparisons were controlled for using
334 the False Discovery Rate (Genovese et al., 2002).

JNeurosci Accepted Manuscript

335

336 **Results**

337

338 **Overabundant emission of laughter-like 50-kHz calls in juvenile *Ube3a*$^{mat-/pat+}$ rats.** Since
339 deficient expressive communication and elevated rates of positive affect are key clinical features of AS,
340 we sought to quantify these characteristics in *Ube3a*$^{mat-/pat+}$ and *Ube3a*$^{mat+/pat+}$ (wildtype) rats. While
341 vocalizations are readily collected during social play, recording USV from multiple interacting animals
342 makes it difficult to determine which animal made each call. We therefore took advantage of the fact that
343 rats emit laughter-like 50-kHz calls when social play is simulated by an experimenter via tickling and
344 other physical maneuverings (Burgdorf and Panksepp, 2001; Burgdorf et al., 2005; Burgdorf et al., 2008;
345 Ishiyama and Brecht, 2016). We implemented a standardized heterospecific play procedure (Figure **1A**)
346 to elicit USV (Figure **1B**) while maintaining full confidence in the identity of the caller and controlling
347 for the level of physical interaction across subjects.

348 We discovered that while both groups increased 50-kHz USV emission across consecutive
349 sessions, *Ube3a*$^{mat-/pat+}$ emitted a substantially elevated level of 50-kHz USV (Figure **1C**;
350 $F_{Genotype(G)}(1,48)=7.351$, $p=0.009$; $F_{Day(D)}(3.007,144.3)=10.82$, $p<0.0001$; $F_{D\times G}(4,192)=1.052$, $p>0.05$). In
351 total, *Ube3a*$^{mat-/pat+}$ emitted an average of 33 ± 5 USV per minute (mean ± S.E.M.), more than twice the
352 rate of controls, which produced an average of 15 ± 3 calls per minute (Figure **1D**; $U=175$, $p=0.007$,
353 $d=0.77$). A closer examination revealed that 50-kHz USV were elevated during the break and belly tickle
354 phases (Figure **1E**; $F_G(1,48)=6.927$, $p=0.011$; $F_{Phase\ (P)}(1.722,82.64)=27.83$, $p<0.0001$; $F_{P\times G}(4,192)=2.075$,
355 $p>0.05$; *post-hoc*: break, $p=0.023$, $d=0.85$; belly tickle, $p=0.023$, $d=0.84$), although calling during the
356 other phases also trended higher, providing strong evidence of elevated positive affect and a high hedonic
357 impact of the assay (neck tickle, $p=0.057$, $d=0.62$; push and drill, $p=0.057$, $d=0.65$; flip over, $p=0.057$,
358 $d=0.69$). There was no effect of sex, nor an interaction with sex, ($p>0.05$) for any parameter.

359 Additionally, 50-kHz USV were more frequently emitted during the anticipation period
360 immediately prior to the play sessions (Figure **1F**; $U=146.5$, $p=0.001$, $d=1.04$). In total, across all four

JNeurosci Accepted Manuscript

361 anticipation timepoints (days 2-5), *Ube3a*$^{mat-/pat+}$ emitted an average of 9 ± 2 USV per minute (mean ±
362 S.E.M.), more than four times the rate of wildtypes, which produced an average of 2 ± 0.4 calls per
363 minute. This indicates that *Ube3a*$^{mat-/pat+}$ predicted the impending onset of play and that the interaction had
364 a high degree of incentive salience.

365 Excessive vocalization by *Ube3a*$^{mat-/pat+}$ rats was specific to 50-kHz USV. Production of short 22-
366 kHz USV, which are emitted in modest amounts during play, was low and did not differ between
367 genotypes (Figure **1G**; $F_G(1,48)=1.771$, $p>0.05$; $F_D(1.825,87.62)=3.160$, $p>0.05$; $F_{D\times G}(4,192)=1.330$,
368 $p>0.05$). Elevated 50-kHz calling by *Ube3a*$^{mat-/pat+}$ was also specific to being provoked by heterospecific
369 play, as 50-kHz and short 22-kHz USV production was normal during exploration of an empty cage
370 (albeit a slight trend toward greater 50-kHz USV; Figure **1H**; 50-kHz, $U=374.5$, $p>0.05$; 22-kHz, $U=433$,
371 $p>0.05$, $d=0.56$) and in response to the acoustic presentation of 50-kHz USV (Figure **1I**; 50-kHz, $U=53$,
372 $p>0.05$; 22-kHz, $U=44.50$, $p>0.05$). No gross abnormalities in call structure were observed. Specifically,
373 50-kHz calls were of normal duration and peak frequency (Figure **1J:** $U=205$, $p>0.05$; Figure **1K:** $U=240$,
374 $p>0.05$; Figure **1N:** $U=52$, $p>0.05$; Figure **1O:** $t(19)=0.3179$, $p>0.05$), suggesting that increased
375 heterospecific play 50-kHz call numbers were not inflated by shorter or broken calls. Duration and peak
376 frequency of 22-kHz USV were also comparable between genotypes (Figure **1L**: $U=12$, $p>0.05$; Figure
377 **1M**: $t(11)=1.699$, $p>0.05$; Figure **1P**: $U=1$, $p>0.05$; Figure **1Q**: $U=1$, $p>0.05$). Since the average duration
378 of the juvenile 22-kHz USV fell short of the usual durations of adult "typical 22-kHz" USV, we herein
379 refer to them as "short 22-kHz" USV.
380

381 **Intact social interest but deficient expression of key social interaction behaviors in juvenile**
382 ***Ube3a*$^{mat-/pat+}$ rats.** We sought to investigate whether elevated 50-kHz USV emission in *Ube3a*$^{mat-/pat+}$ rats
383 was associated with greater social engagement with a conspecific. Starting around two weeks of age, rats
384 play fight with each other by chasing, pouncing, pinning, and wrestling in a manner similar to cats and
385 dogs. Through developmental experience, they learn how to appropriately initiate, engage in, and
386 terminate play bouts with others. In order to more closely examine social behavior and the nuanced

JNeurosci Accepted Manuscript

387 reciprocal interactions of social play, we gave juvenile subjects the opportunity to freely interact with a
388 conspecific (Panksepp, 1981). Despite greater 50-kHz calling during heterospecific play, *Ube3a*$^{mat-/pat+}$ rats
389 showed a normal degree of interest in the stimulus animal, demonstrated by the amounts of time spent
390 social sniffing (Figure **2A**; $t(20)=1.646$, $p>0.05$) and anogenital sniffing (Figure **2B**; $t(20)=0.4457$,
391 $p>0.05$). Putting forth a similar level of investigative effort suggested that *Ube3a*$^{mat-/pat+}$ are just as
392 motivated for social interaction as controls. Levels of self-grooming (Figure **2C**; $U=38$, $p>0.05$) and arena
393 exploration (Figure **2D**; $U=30$, $p>0.05$) were also normal but *Ube3a*$^{mat-/pat+}$ spent markedly less time
394 following or chasing the stimulus rat (Figure **2E**; $U=29$, $p=0.041$, $d=1.11$). The key observation was the
395 reduced time spent rough-and-tumble playing (Figure **2F**; $U=33.50$, $p=0.029$, $d=0.89$) compared to
396 wildtypes. In an attempt to reconcile the near lack of play with intact levels of social interest, we
397 quantified specific components of rough-and-tumble play. While the number of side-to-side social
398 contacts via push pasts were similar across genotypes (Figure **2G**; $t(20)=0.3852$, $p>0.05$), there was a
399 trending reduction in the number of push under or crawl overs (Figure **2H**; $U=31.5$, $p=0.061$, $d=0.89$) and
400 almost a complete lack of pouncing in *Ube3a*$^{mat-/pat+}$ (Figure **2I**; $U=24$, $p=0.008$, $d=1.14$). A separate test
401 of olfaction was used to rule out an olfactory deficit as a confounder of social investigation (Figure **2J**;
402 $F_{Genotype(G)}(1,12)=0.0066$, $p=0.937$; $F_{Scent(S)}(1,12)=14.20$, $p=0.003$; $F_{S\times G}(1,12)=0.0165$, $p=0.900$; *post-hoc*:
403 mat+/pat+, $p=0.035$; mat-/pat+, $p=0.035$).
404
405 **Abnormal gait in *Ube3a*$^{mat-/pat+}$ rats.** In an effort to assess the potential contribution of motor
406 defects to social play behavior, we explored motor dysfunction, which is a core clinical feature of AS
407 prevalent in mouse models (Huang et al., 2013; Leach and Crawley, 2018; Copping and Silverman, 2020)
408 and hypothesized by our group to underlie the open field, rotarod, and marble burying phenotypes of AS
409 mouse models. Previously, we discovered lower open field vertical activity in *Ube3a*$^{mat-/pat+}$ rats while
410 other activity indices were typical (Berg et al., 2020c). Using the DigiGait automated treadmill system,
411 we found that juvenile *Ube3a*$^{mat-/pat+}$ rats displayed robust abnormalities in limb propulsion time,
412 indicating reduced limb strength and less force produced per unit time compared to wildtypes (Figure **3A**;

JNeurosci Accepted Manuscript

$F_{Genotype(G)}(1,44)=0.0684$, $p>0.05$; $F_{Limbs(L)}(1,44)=776.8$, $p<0.0001$; $F_{L\times G}(1,44)=12.80$, $p<0.001$; *post-hoc*: forelimbs, $p=0.030$, $d=0.60$; hindlimbs, $p=0.022$, $d=0.85$; Figure **3B**; $F_G(1,44)=1.012$, $p>0.05$, $F_L(1,44)=687.0$, $p<0.0001$; $F_{L\times G}(1,44)=9.391$, $p=0.004$; *post-hoc*: forelimbs, $p=0.010$, $d=0.65$). No abnormalities in swing time (Figure **3C**; $F_G(1,44)=0.1209$, $p>0.05$, $F_L(1,44)=22.62$, $p<0.0001$; $F_{L\times G}(1,44)=0.2552$, $p>0.05$) or total stride time (Figure **3D**; $F_G(1,44)=0.9166$, $p>0.05$; $F_L(1,44)=13.24$, $p<0.001$; $F_{L\times G}(1,44)=0.7566$, $p>0.05$) were discovered, suggesting that the opposing effects of propulsion and brake time canceled each other out. Stride length was normal, which was surprising given the published Zeno walkway data in humans (Grieco et al., 2018), but lends to the hypothesis that *Ube3a*$^{mat-/pat+}$ have limb weakness since more time was required to produce force for an equal length step (Figure **3F**; $F_G(1,44)=0.9460$, $p>0.05$; $F_L(1,44)=12.70$, $p<0.001$; $F_{L\times G}(1,44)=0.7719$, $p>0.05$). Forelimb stance width was reduced (Figure **3G**; $F_G(1,44)=1.605$, $p>0.05$; $F_L(1,44)=939.0$, $p<0.0001$; $F_{L\times G}(1,44)=12.46$; *post-hoc*: forelimbs, $p=0.022$, $d=0.69$) while an elevated forelimb paw angle indicated greater degree of external rotation and splaying (Figure **3H**; $F_G(1,44)=5.957$, $p=0.019$; $F_L(1,44)=3.726$, $p>0.05$; $F_{L\times G}(1,44)=3.497$, $p>0.05$; *post-hoc*: forelimbs, $p=0.006$, $d=0.86$), which has been associated with ataxia, spinal cord injury, and demyelinating disease (Powell et al., 1999). The observed effects were not attributable to differences in body length (data not shown; $U=244.5$, $p>0.05$) or body width (data not shown; $t(44)=0.2719$, $p>0.05$) and, despite abnormalities in some temporal and postural components of gait, the coordination metric of gait symmetry was unaltered (Figure **3I**; $t(44)=1.023$, $p>0.05$).

Impaired learning and memory in *Ube3a*$^{mat-/pat+}$ rats. Learning and memory impairments, which are characteristic of AS, may hinder the ability of *Ube3a*$^{mat-/pat+}$ rats to learn via developmental experience how to appropriately engage in social interactions. We therefore probed for a juvenile learning and memory deficit using a fear conditioning assay previously used to detect a deficit in adulthood (Dodge et al., 2020). Following successful fear conditioning (Figure **4A**; $F_{Phase(P)}(1,30)=48.47$, $p<0.0001$; $F_{Genotype(G)}(1,30)=0.2203$, $p>0.05$; $F_{P\times G}(1,30)=0.0613$, $p>0.05$; *post-hoc*: mat+/pat+, $p<0.0001$; mat-/pat+, $p<0.001$), juvenile *Ube3a*$^{mat-/pat+}$ displayed normal levels of freezing in response to the training context

JNeurosci Accepted Manuscript

439 (Figure **4B**; U=117.5, p>0.05) but a robust deficit in cued fear memory 48 hrs after training (Figure **4C**;
440 $F_{G}(1,30)=7.395$, $p=0.011$; $F_{P}(1,30)=42.36$, $p<0.0001$; $F_{P\times G}(1,30)=8.699$, $p=0.006$; *post-hoc*: pre-cue,
441 $p>0.05$; cue, $p<0.001$, $d=1.10$). We assessed the potentially confounding variable of impaired
442 sensorimotor processing by measuring the startle response to an intense acoustic stimulus and quantifying
443 the reduction in startle response following prepulses of varying intensities. Both baseline activity (Figure
444 **4D**; $t(22)=1.735$, $p>0.05$) and the acoustic startle response of *Ube3a*$^{mat-/pat+}$ rats were normal (Figure **4E**;
445 $t(22)=1.157$, $p>0.05$), illustrating intact hearing abilities. While there was a significant main effect of
446 genotype on prepulse inhibition, indicative of a sensorimotor gating deficit ($F_{Genotype(G)}(1,22)=4.740$,
447 $p=0.041$, $d=0.88$; $F_{Prepulse(P)}(1.898,41.75)=20.64$, $p<0.0001$; $F_{P\times G}(2,44)=2.127$, $p=0.1312$), *post-hoc* testing
448 revealed no significant difference between groups at any individual prepulse level (Figure **4F**; 74 dB,
449 $p>0.05$, $d=0.25$; 82 dB, $p>0.05$, $d=0.73$; 90 dB, $p>0.05$, $d=1.05$).
450 As an additional assessment of cognitive functioning, we quantified spontaneous alternation
451 during exploration of a Y-maze and found that *Ube3a*$^{mat-/pat+}$ rats displayed reduced spontaneous
452 alternation compared to wildtypes (Figure **4G**; $t(46)=3.115$, $p<0.01$, $d=0.90$). *Ube3a*$^{mat-/pat+}$ rats made 40%
453 more errors (Figure **4H**; $t(46)=3.827$, $p<0.001$, $d=1.10$) and more arm entries (Figure **4I**; $t(46)=3.620$,
454 $p<0.001$, $d=1.04$) despite no difference in the total distance moved (data not shown; Student's t-test:
455 $t(46)=1.721$, $p>0.05$). Taken together, these metrics indicate additional cognitive deficits in the *Ube3a*$^{mat-/pat+}$
456 rats that were not confounded by a locomotor deficiency.
457
458 **Reduced hippocampal long-term potentiation (LTP) in *Ube3a*$^{mat-/pat+}$ rats.** To elucidate the
459 neurobiology underpinning the learning and memory deficits of *Ube3a*$^{mat-/pat+}$ rats, we quantified long-
460 term potentiation (LTP). Previous studies in mouse models of AS have shown that LTP, a major cellular
461 mechanism underlying learning and memory (Collingridge and Isaac, 2003), is impaired (Jiang et al.,
462 1998; van Woerden et al., 2007; Daily et al., 2011). Here, we examined hippocampal LTP in adult
463 *Ube3a*$^{mat-/pat+}$ rats compared to wildtype littermate controls. Since we found hippocampal-dependent
464 contextual fear memory intact at the juvenile age, but a previous report detected a clear deficit in adults

JNeurosci Accepted Manuscript

465 (Dodge et al., 2020), we measured hippocampal LTP in adulthood. Basal synaptic strength (Figure **5A**;
466 $F_{Genotype(G)}(1,92)=0.2013$, $p>0.05$; $F_{Amplitude(A)}(5,111)=94.04$, $p<0.0001$; $F_{G\times A}(5,92)=0.4107$, $p>0.05$) and
467 paired-pulse ratio (Figure **5B**; $F_{G}(1,56)=0.065$, $p>0.05$; $F_{Interval(I)}(3,76)=20.96$, $p<0.0001$;
468 $F_{G\times I}(3,56)=0.0758$, $p>0.05$) were unaltered in *Ube3a*$^{mat-/pat+}$ rats, suggesting no change in baseline
469 excitatory transmission. However, consistent with the mouse models of AS (Jiang et al., 1998; van
470 Woerden et al., 2007; Daily et al., 2011), we found that the magnitude of LTP was reduced in *Ube3a*$^{mat-}$
471 $^{/pat+}$ rats (Figure **5C** and **5D**; $t(25)=4.641$, $p<0.0001$, $d=1.78$), suggesting a putative mechanism underlying
472 impairment of learning and memory (Zucker, 1989; Jiang et al., 1998; Zucker and Regehr, 2002; van
473 Woerden et al., 2007; Daily et al., 2011).
474
475 **Neuroanatomical pathology in *Ube3a*$^{mat-/pat+}$ rats revealed by high-resolution magnetic
476 resonance imaging (MRI).** MRI revealed striking differences in total brain volume at 6.5 months of age,
477 which was decreased by 6.0% in *Ube3a*$^{mat-/pat+}$ rats ($q=0.04$, Figure **6**, Figure **6-1**). The overall brain
478 volume difference was driven by decreases in the hippocampal region (-6.3%, $q=0.04$), brain stem (-
479 5.6%, $q=0.04$), thalamus (-7.7%, $q=0.01$), cerebellum (-9.0%, $q=0.02$), and deep cerebellar nuclei (-
480 12.3%, $q=0.0001$). Additional differences were found throughout the white matter fiber tracts (-7.6%,
481 $q=0.02$), including but not limited to the cerebral peduncle (-7.6%, $q=0.02$), internal capsule (-8.4%,
482 $q=0.02$), and arbor vita of the cerebellum (-11.7%, $q=0.0004$). Moreover, trends were seen in other large
483 white matter structures including the corpus callosum (-6.7%, $q=0.06$) and fornix system (-6.0%, $q=0.09$).
484 A complete list of the regional structural differences in both absolute (mm^3) and relative (% total brain)
485 volume is provided in Figure **6-1**.
486 As we had previously examined *Ube3a*$^{mat-/pat+}$ rats at a juvenile age (postnatal day (PND) 21)
487 (Berg et al., 2020c), we felt an age by genotype comparison was warranted. Figure 6 highlights these
488 changes in eight coronal slices, separately from both the previous work on juvenile rats and from the
489 current data on adults. A combined dataset using both the juvenile and adult data was then used to
490 examine a genotype by age interaction model, which revealed several regions to diverge with age and

JNeurosci Accepted Manuscript

491 genotype: total brain volume (q=0.048), caudoputamen (q=0.03), white matter fiber tracts (q=0.03; Figure
492 **6A**; $F_{Age(A)}(1,97)=546.5$, $p<0.0001$; $F_{Genotype(G)}(1,97)=11.87$, $p<0.001$; $F_{A\times G}(1,97)=10.68$, $p=0.002$; *post-*
493 *hoc*: juvenile, $p>0.05$; adult, $p<0.0001$, $d=1.02$), hypothalamus (q=0.046; Figure **6B**; $F_A(1,97)=460.2$,
494 $p<0.0001$; $F_G(1,97)=5.081$, $p=0.026$; $F_{A\times G}(1,97)=8.760$, $p=0.004$; *post-hoc*: juvenile, $p>0.05$; adult,
495 $p=0.001$, $d=0.82$), hippocampal region (q=0.046; Figure **6C**; $F_A(1,97)=434.4$, $p<0.0001$; $F_G(1,97)=10.89$,
496 $p=0.001$; $F_{A\times G}(1,97)=8.760$, $p=0.004$; *post-hoc*: juvenile, $p>0.05$; adult, $p<0.0001$, $d=1.02$), and thalamus
497 (q=0.02; Figure **6D**; $F_A(1,97)=430.2$, $p<0.0001$; $F_G(1,97)=11.14$, $p=0.001$; $F_{A\times G}(1,97)=14.96$, $p<0.001$;
498 *post-hoc*: juvenile, $p>0.05$; adult, $p<0.0001$, $d=1.22$). A full list of the regional genotype by age
499 interactions is located in Figure **6-2**. Voxelwise changes were also found throughout the brain of adult
500 *Ube3a*$^{mat-/pat+}$ rats compared to the juvenile age. The changes in the adults were substantially larger,
501 signaling a more severe neuroanatomical phenotype with age (Figure **6**).
502
503 **Discussion**
504
505 Indispensable to therapeutic development are *in vivo* studies utilizing preclinical model systems.
506 While mice have prevailed as the animal model of AS in recent decades (Jiang et al., 1998), the *Ube3a*$^{mat-}$
507 $^{/pat+}$ rat offers a unique and suitable system for investigating certain complexities of the human AS
508 phenotype, particularly social communication and affect (Brudzynski, 2013; Wöhr and Schwarting, 2013;
509 Burgdorf et al., 2020; Burke et al., 2017; Homberg et al., 2017; Netser et al., 2020). Our discovery of
510 excessive laughter-like 50-kHz USV is the first report of this affective outcome measure in a model of
511 AS, mirroring the affected population. Moreover, reduced social play, atypical gait, impaired cognition,
512 and anatomical and cellular physiology anomalies were easily detected in this model.
513 We leveraged our model species to discover that *Ube3a*$^{mat-/pat+}$ rats produced an overabundance of
514 50-kHz vocalizations, which reflect a positive affective state and have been referred to as rat laughter
515 (Panksepp and Burgdorf, 2000; Panksepp, 2005), as well as a trend of elevated laughter-like 50-kHz USV
516 without provocation. Excessive 50-kHz USV, suggestive of enhanced 'wanting' and 'liking' the

JNeurosci Accepted Manuscript

517 interaction (Berridge, 2009; Berridge and Aldridge, 2009; Berridge et al., 2009; Okabe et al., 2021),
518 closely aligns with the AS profile of a happy disposition and easily provoked laughter. To our knowledge,
519 this is the first report of this method being used in a genetic rat model of a neurological disorder.

520 Exaggerated 50-kHz calling could suggest enhanced effort to elicit social interaction or may be
521 unrelated to the social component of heterospecific play, potentially a neurobiological consequence of a
522 disinhibited vocal production pathway. AS is typified by laughter that is easily provoked regardless of
523 stimuli valence. The phenotype may also reflect enhanced sensitivity to tactile stimulation. Deriving
524 greater reward from physical interactions could explain typical levels of social investigation in the
525 reciprocal interaction test but reduced social approach in three-chambered and USV playback assays, as
526 well as the disinhibition of social interactions in the clinical population. One limitation of our USV
527 analysis was the lack of acoustic feature quantification for the calls evoked by heterospecific play. We
528 did, however, subsequently carry out this analysis for all other USV assays and found no genotype effect
529 on call features.

530 Juvenile social play is a critical way that rats develop social competence and learn how to
531 appropriately engage and communicate with others, analogous to play in young children (Hofer and Shair,
532 1978; Panksepp and Beatty, 1980; Panksepp, 1981; Brudzynski, 2009, 2013; Argue and McCarthy, 2015).
533 *Ube3a*$^{mat-/pat+}$ rats were interested in a novel partner but did not engage in rough-and-tumble play
534 behaviors characteristic of the species, albeit specific to sex and strain. Our finding of no sex difference in
535 rough-and-tumble play aligns with previous reports which also used pre-test social isolation to motivate
536 the subjects to play (Veenema et al., 2013; Bredewold et al., 2014; Bredewold et al., 2015; Reppucci et
537 al., 2018; Kisko et al., 2020). In contrast with studies on mouse models of AS using the three-chambered
538 social approach task (Jamal et al., 2017; Kumar et al., 2019; Perrino et al., 2020; Dutta and Crawley,
539 2020), which have reported contradictory social deficits and "hypersociability," the rat model displayed a
540 typical level of social investigation.

541 Movement disorders (Wheeler et al., 2017) are a hallmark feature of AS, with gait ataxia being
542 one of the most common issues. While the deficits of *Ube3a*$^{mat-/pat+}$ rats were not obvious to the eye, subtle

JNeurosci Accepted Manuscript

543 aberrations in stance and paw placement, paired with abnormal braking and propelling, reflect impaired
544 motor coordination. All of this evidence suggests that altered postures affect motor dynamics which
545 results in the gait patterns exhibited by AS individuals and *Ube3a*$^{mat-/pat+}$ rats. The limb weakness
546 indicated by our gait analysis aligns with the reduced rearing previously observed (Berg et al., 2020c).

547 We discovered and report for the first time, to our knowledge, of long-term potentiation (LTP)
548 deficits in this rat model (Jiang et al., 1998; Weeber et al., 2003; van Woerden et al., 2007; Filonova et al.,
549 2014; Ciarlone et al., 2016), which provides a putative cellular signaling mechanism underlying the
550 learning and memory impairments reported herein and previously (Berg et al., 2020c; Dodge et al., 2020).
551 Juvenile *Ube3a*$^{mat-/pat+}$ rats exhibited deficits in cued fear memory 48 hours post-training, which extends
552 the previous finding by Dodge et al. of deficient contextual and cued fear conditioning in adults 72 hours
553 post-training (Dodge et al., 2020). We ruled out impaired sensorimotor abilities as a confounding variable
554 since the acoustic startle response was unaffected.

555 Pronounced deficits in adulthood are supported by neuroimaging. Previously, we discovered a
556 variety of trending volumetric abnormalities at PND 21 (Berg et al., 2020c), however, these new data
557 show more substantial reductions in adults throughout the brain, highlighting a more severe
558 neuroanatomical phenotype with age. Reduced total brain volume may indicate a loss of cellular volume
559 or dendritic complexity over time, and the drastic volume loss in fiber tracts could indicate a loss in
560 axonal numbers, axonal volume, or myelination. In a mouse model of AS, white matter loss was found to
561 play a large role in the overall microcephaly observed (Judson et al., 2017), with an 11% loss in the
562 corpus callosum making it the most affected white matter structure. *Ube3a*$^{mat-/pat+}$ rats showed a trend
563 towards reduced corpus callosum volume (-6.7%), but the largest white matter deficits were cerebellar. In
564 alignment with Judson et al.'s (2017) study in mice, the reduced fiber tracts volume was also
565 disproportionate to the overall brain volume loss, confirming that white matter development plays the
566 major role in the impaired brain growth in AS. Additionally, the 9% decrease in cerebellum size was
567 consistent with cortical loss (-9%), but there was a disproportionate reduction in arbor vitae and deep
568 cerebellar nuclei volume, indicating that the outputs of the cerebellum are impaired.

JNeurosci Accepted Manuscript

569 GABAergic neuron loss (Judson et al., 2016) and decreased tonic inhibition in cerebellar granule
570 cells (Egawa et al., 2012) underlie the theory of brain dysfunction in AS, and hypotheses addressing the
571 theory of reduced inhibitory tone are being pursued for small molecule development (Ciarlone et al.,
572 2017). The present results are congruent with this overarching mechanism theory of AS, loss of inhibitory
573 tone. Emission of 50-kHz USV induced by heterospecific play is associated with dopamine release in the
574 nucleus accumbens/ventral striatum. These calls have been considered as “joy,” “euphoria,” and
575 “laughter,” supported by behavioral pharmacology showing increased 50-kHz USV resulting from
576 amphetamine administration (Brudzynski, 2013, 2015; Wöhr, 2021). Both vocalizations and gait require
577 fine motor control and thus striatal and motivational components support aberrant frontal-striatal
578 circuitry. Interestingly, the ventral striatum and “reward” associated substrates of the basal ganglia have
579 inhibitory projections, in line with overall theories of AS regarding inhibitory loss.

580 While gross and fine movement are complicated multi-system physiological processes, AS
581 individuals show ataxic movements in both upper and lower limbs and aberrant gait, suggesting the
582 particular involvement of the cerebellum. This was corroborated here and in earlier work by the large
583 reductions in cerebellar nuclei size, which is consistent with our overarching mechanistic hypothesis since
584 Purkinje cell neurons to the deep cerebellar nuclei modulate excitation via inhibition and Egawa et al.
585 (2012) highlighted decreased cerebellar granule cells in AS. Utilizing conditional *Ube3a* mouse models to
586 identify the neural substrates of circuit hyperexcitability in AS, Judson et al. (2016) provided compelling
587 evidence that GABAergic, but not glutamatergic, *Ube3a* loss is responsible for mediating the EEG
588 abnormalities and seizures of AS. Previously, we reproduced and extended Judson et al.’s. (2016) data
589 (Copping and Silverman, 2021) and our hypothesis is that this mechanism extends to social
590 communication, cognitive phenotypes, and impaired gait outcomes, as each shares components of
591 learning and motivation. The loss of brain volume in regions dense with inhibitory neurons seen herein
592 provides further corroborative evidence that GABAergic tone underlies functional outcomes. Independent
593 corroboration comes from ErbB inhibitors, which have been reported to reverse LTP deficits in AS model
594 mice (Kaphzan et al., 2012). While glutamate receptor expression and function were unaltered in *Ube3a*

JNeurosci Accepted Manuscript

595 mice (Kaphzan et al., 2012; Judson et al., 2016), ErbB signaling was shown to rescue LTP impairments in
596 *Ube3a* mice via an increase in inhibitory synaptic transmission, corroborating our core overarching
597 mechanism of reduced inhibitory tone.

598 In conclusion, we discovered that *Ube3a*$^{mat-/pat+}$ rats exhibited interest in a social partner but
599 expressed an atypically high level of laughter-like vocalizations. Deficits in other AS-relevant domains
600 were also discovered, including gait and cognition, and reduced hippocampal LTP. Future lines of
601 investigation will assess the circuitry and mechanisms underlying the excessive laughter-like USV and
602 social-cognitive anomalies in USV reception, in addition to pursuing other neurobiological endpoints.
603 Overall, our results indicate that the deletion of maternal *Ube3a* in the rat creates a sophisticated rodent
604 model with high face validity to the human AS phenotype. In the pursuit of effective therapeutics, it is
605 essential to be equipped with a diverse set of behavioral outcome measures and neurological biomarkers
606 by which to assess efficacy. Taken together, we demonstrate that the *Ube3a*$^{mat-/pat+}$ rat offers numerous
607 potential outcome measures that are detectable throughout the lifespan.

608

609 **References**

610 Adhikari, Copping NA, Beegle, Cameron DL, Deng P, O'Geen H, Segal DJ, Fink KD, Silverman JL, JS
611 A (2021) Functional rescue in an Angelman syndrome model following treatment with lentivector
612 transduced hematopoietic stem cells. Human Molecular Genetics In press.

613 Adhikari A, Copping NA, Onaga B, Pride MC, Coulson RL, Yang M, Yasui DH, LaSalle JM, Silverman
614 JL (2018) Cognitive Deficits in the Snord116 Deletion Mouse Model for Prader-Willi Syndrome.
615 Neurobiol Learn Mem.

616 Albrecht U, Sutcliffe JS, Cattanach BM, Beechey CV, Armstrong D, Eichele G, Beaudet AL (1997)
617 Imprinted expression of the murine Angelman syndrome gene, Ube3a, in hippocampal and
618 Purkinje neurons. Nat Genet 17:75-78.

619 Argue KJ, McCarthy MM (2015) Utilization of same- vs. mixed-sex dyads impacts the observation of sex
620 differences in juvenile social play behavior. Curr Neurobiol 6:17-23.

JNeurosci Accepted Manuscript

621 Avants BB, Tustison NJ, Song G, Cook PA, Klein A, Gee JC (2011) A reproducible evaluation of ANTs
622 similarity metric performance in brain image registration. Neuroimage 54:2033-2044.
623 Bailus BJ, Pyles B, McAlister MM, O'Geen H, Lockwood SH, Adams AN, Nguyen JT, Yu A, Berman
624 RF, Segal DJ (2016) Protein Delivery of an Artificial Transcription Factor Restores Widespread
625 Ube3a Expression in an Angelman Syndrome Mouse Brain. Mol Ther 24:548-555.
626 Berg EL, Ching TM, Bruun DA, Rivera JK, Careaga M, Ellegood J, Lerch JP, Wöhr M, Lein PJ,
627 Silverman JL (2020a) Translational outcomes relevant to neurodevelopmental disorders
628 following early life exposure of rats to chlorpyrifos. J Neurodev Disord 12:40.
629 Berg EL, Pedersen LR, Pride MC, Petkova SP, Patten KT, Valenzuela AE, Wallis C, Bein KJ, Wexler A,
630 Lein PJ, Silverman JL (2020b) Developmental exposure to near roadway pollution produces
631 behavioral phenotypes relevant to neurodevelopmental disorders in juvenile rats. Transl
632 Psychiatry 10:289.
633 Berg EL, Copping NA, Rivera JK, Pride MC, Careaga M, Bauman MD, Berman RF, Lein PJ, Harony-
634 Nicolas H, Buxbaum JD, Ellegood J, Lerch JP, Wöhr M, Silverman JL (2018) Developmental
635 social communication deficits in the Shank3 rat model of phelan-mcdermid syndrome and autism
636 spectrum disorder. Autism Res 11:587-601.
637 Berg EL et al. (2020c) Translational outcomes in a full gene deletion of ubiquitin protein ligase E3A rat
638 model of Angelman syndrome. Transl Psychiatry 10:39.
639 Berridge KC (2009) 'Liking' and 'wanting' food rewards: brain substrates and roles in eating disorders.
640 Physiol Behav 97:537-550.
641 Berridge KC, Aldridge JW (2009) Decision Utility, Incentive Salience, and Cue-Triggered "Wanting".
642 Oxf Ser Soc Cogn Soc Neurosci 2009:509-533.
643 Berridge KC, Robinson TE, Aldridge JW (2009) Dissecting components of reward: 'liking', 'wanting', and
644 learning. Curr Opin Pharmacol 9:65-73.
645 Bird LM (2014) Angelman syndrome: review of clinical and molecular aspects. Appl Clin Genet 7:93-
646 104.

JNeurosci Accepted Manuscript

647 Bishop J, Feintuch A, Bock NA, Nieman B, Dazai J, Davidson L, Henkelman RM (2006) Retrospective
648 gating for mouse cardiac MRI. Magn Reson Med 55:472-477.
649 Blanchard RJ, Blanchard DC, Agullana R, Weiss SM (1991) Twenty-two kHz alarm cries to presentation
650 of a predator, by laboratory rats living in visible burrow systems. Physiol Behav 50:967-972.
651 Bock NA, Nieman BJ, Bishop JB, Mark Henkelman R (2005) In vivo multiple-mouse MRI at 7 Tesla.
652 Magn Reson Med 54:1311-1316.
653 Born HA, Dao AT, Levine AT, Lee WL, Mehta NM, Mehra S, Weeber EJ, Anderson AE (2017) Strain-
654 dependence of the Angelman Syndrome phenotypes in Ube3a maternal deficiency mice. Sci Rep
655 7:8451.
656 Braun MD, Kisko TM, Vecchia DD, Andreatini R, Schwarting RKW, Wöhr M (2018) Sex-specific
657 effects of Cacna1c haploinsufficiency on object recognition, spatial memory, and reversal
658 learning capabilities in rats. Neurobiology of learning and memory 155:543-555.
659 Bredewold R, Nascimento NF, Ro GS, Cieslewski SE, Reppucci CJ, Veenema AH (2018) Involvement of
660 dopamine, but not norepinephrine, in the sex-specific regulation of juvenile socially rewarding
661 behavior by vasopressin. Neuropsychopharmacology 43:2109-2117.
662 Brudzynski SM (2009) Communication of adult rats by ultrasonic vocalization: biological,
663 sociobiological, and neuroscience approaches. ILAR J 50:43-50.
664 Brudzynski SM (2013) Ethotransmission: communication of emotional states through ultrasonic
665 vocalization in rats. Curr Opin Neurobiol 23:310-317.
666 Brudzynski SM (2015) Pharmacology of Ultrasonic Vocalizations in adult Rats: Significance, Call
667 Classification and Neural Substrate. Curr Neuropharmacol 13:180-192.
668 Burgdorf J, Panksepp J (2001) Tickling induces reward in adolescent rats. Physiol Behav 72:167-173.
669 Burgdorf J, Panksepp J, Brudzynski SM, Kroes R, Moskal JR (2005) Breeding for 50-kHz positive
670 affective vocalization in rats. Behav Genet 35:67-72.

JNeurosci Accepted Manuscript

671 Burgdorf J, Kroes RA, Moskal JR, Pfaus JG, Brudzynski SM, Panksepp J (2008) Ultrasonic vocalizations
672 of rats (Rattus norvegicus) during mating, play, and aggression: Behavioral concomitants,
673 relationship to reward, and self-administration of playback. J Comp Psychol 122:357-367.
674 Burgdorf JS, Brudzynski SM, Moskal JR (2020) Using rat ultrasonic vocalization to study the
675 neurobiology of emotion: from basic science to the development of novel therapeutics for
676 affective disorders. Curr Opin Neurobiol 60:192-200.
677 Burke CJ, Kisko TM, Swiftwolfe H, Pellis SM, Euston DR (2017) Specific 50-kHz vocalizations are
678 tightly linked to particular types of behavior in juvenile rats anticipating play. PLoS One
679 12:e0175841.
680 Cassidy SB, Dykens E, Williams CA (2000) Prader-Willi and Angelman syndromes: sister imprinted
681 disorders. Am J Med Genet 97:136-146.
682 Ciarlone SL, Grieco JC, D'Agostino DP, Weeber EJ (2016) Ketone ester supplementation attenuates
683 seizure activity, and improves behavior and hippocampal synaptic plasticity in an Angelman
684 syndrome mouse model. Neurobiol Dis 96:38-46.
685 Ciarlone SL, Wang X, Rogawski MA, Weeber EJ (2017) Effects of the synthetic neurosteroid ganaxolone
686 on seizure activity and behavioral deficits in an Angelman syndrome mouse model.
687 Neuropharmacology 116:142-150.
688 Collingridge GL, Isaac JT (2003) Functional roles of protein interactions with AMPA and kainate
689 receptors. Neurosci Res 47:3-15.
690 Collins DL, Neelin P, Peters TM, Evans AC (1994) Automatic 3D intersubject registration of MR
691 volumetric data in standardized Talairach space. J Comput Assist Tomogr 18:192-205.
692 Copping, Silverman (2020) Abnormal electrophysiological phenotypes and sleep deficits in a mouse
693 model of Angelman Syndrome. Molecular Autism In press.
694 Copping NA, Silverman JL (2021) Abnormal electrophysiological phenotypes and sleep deficits in a
695 mouse model of Angelman Syndrome. Mol Autism 12:9.

JNeurosci Accepted Manuscript

696 Copping NA, Christian SGB, Ritter DJ, Islam MS, Buscher N, Zolkowska D, Pride MC, Berg EL,
697 LaSalle JM, Ellegood J, Lerch JP, Reiter LT, Silverman JL, Dindot SV (2017) Neuronal
698 overexpression of Ube3a isoform 2 causes behavioral impairments and neuroanatomical
699 pathology relevant to 15q11.2-q13.3 duplication syndrome. Hum Mol Genet 26:3995-4010.
700 Daily JL, Nash K, Jinwal U, Golde T, Rogers J, Peters MM, Burdine RD, Dickey C, Banko JL, Weeber
701 EJ (2011) Adeno-associated virus-mediated rescue of the cognitive defects in a mouse model for
702 Angelman syndrome. PLoS One 6:e27221.
703 Dodge A, Peters MM, Greene HE, Dietrick C, Botelho R, Chung D, Willman J, Nenninger AW, Ciarlone
704 S, Kamath SG, Houdek P, Sumova A, Anderson AE, Dindot SV, Berg EL, O'Geen H, Segal DJ,
705 Silverman JL, Weeber EJ, Nash KR (2020) Generation of a Novel Rat Model of Angelman
706 Syndrome with a Complete Ube3a Gene Deletion. Autism Res 13:397-409.
707 Dorr AE, Lerch JP, Spring S, Kabani N, Henkelman RM (2008) High resolution three-dimensional brain
708 atlas using an average magnetic resonance image of 40 adult C57Bl/6J mice. Neuroimage 42:60-
709 69.
710 Dutta R, Crawley JN (2020) Behavioral Evaluation of Angelman Syndrome Mice at Older Ages.
711 Neuroscience 445:163-171.
712 Egawa K, Kitagawa K, Inoue K, Takayama M, Takayama C, Saitoh S, Kishino T, Kitagawa M, Fukuda A
713 (2012) Decreased tonic inhibition in cerebellar granule cells causes motor dysfunction in a mouse
714 model of Angelman syndrome. Sci Transl Med 4:163ra157.
715 Ellenbroek B, Youn J (2016) Rodent models in neuroscience research: is it a rat race? Dis Model Mech
716 9:1079-1087.
717 Fendt M, Brosch M, Wernecke KEA, Willadsen M, Wöhr M (2018) Predator odour but not TMT induces
718 22-kHz ultrasonic vocalizations in rats that lead to defensive behaviours in conspecifics upon
719 replay. Scientific reports 8:11041.
720 Fernandez M, Mollinedo-Gajate I, Penagarikano O (2018) Neural Circuits for Social Cognition:
721 Implications for Autism. Neuroscience 370:148-162.

JNeurosci Accepted Manuscript

722 Filonova I, Trotter JH, Banko JL, Weeber EJ (2014) Activity-dependent changes in MAPK activation in
723 the Angelman Syndrome mouse model. Learn Mem 21:98-104.
724 Genovese CR, Lazar NA, Nichols T (2002) Thresholding of statistical maps in functional neuroimaging
725 using the false discovery rate. NeuroImage 15:870-878.
726 Gentile JK, Tan WH, Horowitz LT, Bacino CA, Skinner SA, Barbieri-Welge R, Bauer-Carlin A, Beaudet
727 AL, Bichell TJ, Lee HS, Sahoo T, Waisbren SE, Bird LM, Peters SU (2010) A
728 neurodevelopmental survey of Angelman syndrome with genotype-phenotype correlations. J Dev
729 Behav Pediatr 31:592-601.
730 Grieco JC, Gouelle A, Weeber EJ (2018) Identification of spatiotemporal gait parameters and pressure-
731 related characteristics in children with Angelman syndrome: A pilot study. J Appl Res Intellect
732 Disabil 31:1219-1224.
733 Hammerschmidt K, Reisinger E, Westekemper K, Ehrenreich L, Strenzke N, Fischer J (2012) Mice do
734 not require auditory input for the normal development of their ultrasonic vocalizations. BMC
735 Neurosci 13:40.
736 Harony-Nicolas H, Kay M, du Hoffmann J, Klein ME, Bozdagi-Gunal O, Riad M, Daskalakis NP, Sonar
737 S, Castillo PE, Hof PR, Shapiro ML, Baxter MG, Wagner S, Buxbaum JD (2017) Oxytocin
738 improves behavioral and electrophysiological deficits in a novel Shank3-deficient rat. Elife 6.
739 Hofer MA, Shair H (1978) Ultrasonic vocalization during social interaction and isolation in 2-weeek-old
740 rats. Dev Psychobiol 11:495-504.
741 Hofer MA, Shair HN, Brunelli SA (2002) Ultrasonic vocalizations in rat and mouse pups. Current
742 protocols in neuroscience / editorial board, Jacqueline N Crawley [et al] Chapter 8:Unit 8 14.
743 Homberg JR, Wöhr M, Alenina N (2017) Comeback of the Rat in Biomedical Research. ACS Chem
744 Neurosci 8:900-903.
745 Huang HS, Burns AJ, Nonneman RJ, Baker LK, Riddick NV, Nikolova VD, Riday TT, Yashiro K,
746 Philpot BD, Moy SS (2013) Behavioral deficits in an Angelman syndrome model: effects of
747 genetic background and age. Behav Brain Res 243:79-90.

JNeurosci Accepted Manuscript

748 Ishiyama S, Brecht M (2016) Neural correlates of ticklishness in the rat somatosensory cortex. Science
749 354:757-760.
750 Jamal I, Kumar V, Vatsa N, Shekhar S, Singh BK, Sharma A, Jana NR (2017) Rescue of altered HDAC
751 activity recovers behavioural abnormalities in a mouse model of Angelman syndrome. Neurobiol
752 Dis 105:99-108.
753 Jiang YH, Armstrong D, Albrecht U, Atkins CM, Noebels JL, Eichele G, Sweatt JD, Beaudet AL (1998)
754 Mutation of the Angelman ubiquitin ligase in mice causes increased cytoplasmic p53 and deficits
755 of contextual learning and long-term potentiation. Neuron 21:799-811.
756 Jiang YH, Pan Y, Zhu L, Landa L, Yoo J, Spencer C, Lorenzo I, Brilliant M, Noebels J, Beaudet AL
757 (2010) Altered ultrasonic vocalization and impaired learning and memory in Angelman syndrome
758 mouse model with a large maternal deletion from Ube3a to Gabrb3. PLoS One 5:e12278.
759 Judson MC, Burette AC, Thaxton CL, Pribisko AL, Shen MD, Rumple AM, Del Cid WA, Paniagua B,
760 Styner M, Weinberg RJ, Philpot BD (2017) Decreased Axon Caliber Underlies Loss of Fiber
761 Tract Integrity, Disproportional Reductions in White Matter Volume, and Microcephaly in
762 Angelman Syndrome Model Mice. J Neurosci 37:7347-7361.
763 Judson MC, Wallace ML, Sidorov MS, Burette AC, Gu B, van Woerden GM, King IF, Han JE, Zylka
764 MJ, Elgersma Y, Weinberg RJ, Philpot BD (2016) GABAergic Neuron-Specific Loss of Ube3a
765 Causes Angelman Syndrome-Like EEG Abnormalities and Enhances Seizure Susceptibility.
766 Neuron 90:56-69.
767 Kaphzan H, Hernandez P, Jung JI, Cowansage KK, Deinhardt K, Chao MV, Abel T, Klann E (2012)
768 Reversal of impaired hippocampal long-term potentiation and contextual fear memory deficits in
769 Angelman syndrome model mice by ErbB inhibitors. Biol Psychiatry 72:182-190.
770 Kisko TM, Euston DR, Pellis SM (2015) Are 50-khz calls used as play signals in the playful interactions
771 of rats? III. The effects of devocalization on play with unfamiliar partners as juveniles and as
772 adults. Behav Processes 113:113-121.

JNeurosci Accepted Manuscript

773 Kisko TM, Wöhr M, Pellis VC, Pellis SM (2017) From Play to Aggression: High-Frequency 50-kHz
774 Ultrasonic Vocalizations as Play and Appeasement Signals in Rats. Curr Top Behav Neurosci
775 30:91-108.
776 Kisko TM, Braun MD, Michels S, Witt SH, Rietschel M, Culmsee C, Schwarting RKW, Wöhr M (2018a)
777 Cacna1c haploinsufficiency leads to pro-social 50-kHz ultrasonic communication deficits in rats.
778 Disease models & mechanisms 11.
779 Kisko TM, Braun MD, Michels S, Witt SH, Rietschel M, Culmsee C, Schwarting RKW, Wöhr M (2018b)
780 Sex-dependent effects of Cacna1c haploinsufficiency on juvenile social play behavior and pro-
781 social 50-kHz ultrasonic communication in rats. Genes Brain Behav:e12552.
782 Kondrakiewicz K, Kostecki M, Szadzinska W, Knapska E (2019) Ecological validity of social interaction
783 tests in rats and mice. Genes Brain Behav 18:e12525.
784 Ku CS, Loy EY, Pawitan Y, Chia KS (2010) The pursuit of genome-wide association studies: where are
785 we now? J Hum Genet 55:195-206.
786 Ku KM, Weir RK, Silverman JL, Berman RF, Bauman MD (2016) Behavioral Phenotyping of Juvenile
787 Long-Evans and Sprague-Dawley Rats: Implications for Preclinical Models of Autism Spectrum
788 Disorders. PLoS One 11:e0158150.
789 Kumar V, Joshi T, Vatsa N, Singh BK, Jana NR (2019) Simvastatin Restores HDAC1/2 Activity and
790 Improves Behavioral Deficits in Angelman Syndrome Model Mouse. Front Mol Neurosci 12:1-
791 11.
792 Leach PT, Crawley JN (2018) Touchscreen learning deficits in Ube3a, Ts65Dn and Mecp2 mouse models
793 of neurodevelopmental disorders with intellectual disabilities. Genes Brain Behav 17:e12452.
794 Lerch JP, Sled JG, Henkelman RM (2011) MRI phenotyping of genetically altered mice. Methods Mol
795 Biol 711:349-361.
796 Lerch JP, Carroll JB, Spring S, Bertram LN, Schwab C, Hayden MR, Henkelman RM (2008a) Automated
797 deformation analysis in the YAC128 Huntington disease mouse model. NeuroImage 39:32-39.

JNeurosci Accepted Manuscript

798 Lerch JP, Pruessner J, Zijdenbos AP, Collins DL, Teipel SJ, Hampel H, Evans AC (2008b) Automated
799 cortical thickness measurements from MRI can accurately separate Alzheimer's patients from
800 normal elderly controls. Neurobiol Aging 29:23-30.
801 Lerch JP, Carroll JB, Dorr A, Spring S, Evans AC, Hayden MR, Sled JG, Henkelman RM (2008c)
802 Cortical thickness measured from MRI in the YAC128 mouse model of Huntington's disease.
803 NeuroImage 41:243-251.
804 Lopuch S, Popik P (2011) Cooperative behavior of laboratory rats (Rattus norvegicus) in an instrumental
805 task. J Comp Psychol 125:250-253.
806 Meaney MJ, Stewart J (1981) Neonatal-androgens influence the social play of prepubescent rats.
807 Hormones and behavior 15:197-213.
808 Meng L, Ward AJ, Chun S, Bennett CF, Beaudet AL, Rigo F (2015) Towards a therapy for Angelman
809 syndrome by targeting a long non-coding RNA. Nature 518:409-412.
810 Netser S, Meyer A, Magalnik H, Zylbertal A, de la Zerda SH, Briller M, Bizer A, Grinevich V, Wagner S
811 (2020) Distinct dynamics of social motivation drive differential social behavior in laboratory rat
812 and mouse strains. Nat Commun 11:5908.
813 Nieman BJ, Shyu JY, Rodriguez JJ, Garcia AD, Joyner AL, Turnbull DH (2010) In vivo MRI of neural
814 cell migration dynamics in the mouse brain. NeuroImage 50:456-464.
815 Nieman BJ, van Eede MC, Spring S, Dazai J, Henkelman RM, Lerch JP (2018) MRI to Assess
816 Neurological Function. Curr Protoc Mouse Biol 8:e44.
817 Okabe S, Takayanagi Y, Yoshida M, Onaka T (2021) Post-weaning stroking stimuli induce affiliative
818 behavior toward humans and influence brain activity in female rats. Sci Rep 11:3805.
819 Panksepp J (1981) The ontogeny of play in rats. Dev Psychobiol 14:327-332.
820 Panksepp J (2005) Psychology. Beyond a joke: from animal laughter to human joy? Science 308:62-63.
821 Panksepp J, Beatty WW (1980) Social deprivation and play in rats. Behav Neural Biol 30:197-206.

JNeurosci Accepted Manuscript

822 Panksepp J, Burgdorf J (2000) 50-kHz chirping (laughter?) in response to conditioned and unconditioned
823 tickle-induced reward in rats: effects of social housing and genetic variables. Behav Brain Res
824 115:25-38.
825 Parker CC, Chen H, Flagel SB, Geurts AM, Richards JB, Robinson TE, Solberg Woods LC, Palmer AA
826 (2014) Rats are the smart choice: Rationale for a renewed focus on rats in behavioral genetics.
827 Neuropharmacology 76 Pt B:250-258.
828 Pellis SM, Pellis VC (1998) Play fighting of rats in comparative perspective: a schema for
829 neurobehavioral analyses. Neuroscience and biobehavioral reviews 23:87-101.
830 Pellis SM, Pellis VC (2017) What is play fighting and what is it good for? Learn Behav 45:355-366.
831 Portfors CV (2007) Types and functions of ultrasonic vocalizations in laboratory rats and mice. J Am
832 Assoc Lab Anim Sci 46:28-34.
833 Portfors CV, Perkel DJ (2014) The role of ultrasonic vocalizations in mouse communication. Curr Opin
834 Neurobiol 28:115-120.
835 Powell E, Anch AM, Dyche J, Bloom C, Richtert RR (1999) The splay angle: A new measure for
836 assessing neuromuscular dysfunction in rats. Physiol Behav 67:819-821.
837 Reppucci CJ, Brown LA, Chambers AQ, Veenema AH (2020) Wistar rats and C57BL/6 mice differ in
838 their motivation to seek social interaction versus food in the Social versus Food Preference Test.
839 Physiol Behav 227:113162.
840 Rygula R, Pluta H, Popik P (2012) Laughing rats are optimistic. PloS one 7:e51959.
841 Sadananda M, Wöhr M, Schwarting RK (2008) Playback of 22-kHz and 50-kHz ultrasonic vocalizations
842 induces differential c-fos expression in rat brain. Neurosci Lett 435:17-23.
843 Schwarting RK, Jegan N, Wöhr M (2007) Situational factors, conditions and individual variables which
844 can determine ultrasonic vocalizations in male adult Wistar rats. Behav Brain Res 182:208-222.
845 Spencer Noakes TL, Henkelman RM, Nieman BJ (2017) Partitioning k-space for cylindrical three-
846 dimensional rapid acquisition with relaxation enhancement imaging in the mouse brain. NMR
847 Biomed 30.

JNeurosci Accepted Manuscript

848 Steadman PE, Ellegood J, Szulc KU, Turnbull DH, Joyner AL, Henkelman RM, Lerch JP (2014) Genetic
849 effects on cerebellar structure across mouse models of autism using a magnetic resonance
850 imaging atlas. Autism Res 7:124-137.
851 Tan WH, Bird LM (2016) Angelman syndrome: Current and emerging therapies in 2016. Am J Med
852 Genet C Semin Med Genet 172:384-401.
853 Tan WH, Bacino CA, Skinner SA, Anselm I, Barbieri-Welge R, Bauer-Carlin A, Beaudet AL, Bichell TJ,
854 Gentile JK, Glaze DG, Horowitz LT, Kothare SV, Lee HS, Nespeca MP, Peters SU, Sahoo T,
855 Sarco D, Waisbren SE, Bird LM (2011) Angelman syndrome: Mutations influence features in
856 early childhood. Am J Med Genet A 155A:81-90.
857 van Woerden GM, Harris KD, Hojjati MR, Gustin RM, Qiu S, de Avila Freire R, Jiang YH, Elgersma Y,
858 Weeber EJ (2007) Rescue of neurological deficits in a mouse model for Angelman syndrome by
859 reduction of alphaCaMKII inhibitory phosphorylation. Nat Neurosci 10:280-282.
860 Varlinskaya EI, Spear LP (2008) Social interactions in adolescent and adult Sprague-Dawley rats: impact
861 of social deprivation and test context familiarity. Behav Brain Res 188:398-405.
862 Weeber EJ, Jiang YH, Elgersma Y, Varga AW, Carrasquillo Y, Brown SE, Christian JM, Mirnikjoo B,
863 Silva A, Beaudet AL, Sweatt JD (2003) Derangements of hippocampal calcium/calmodulin-
864 dependent protein kinase II in a mouse model for Angelman mental retardation syndrome. J
865 Neurosci 23:2634-2644.
866 Wheeler AC, Sacco P, Cabo R (2017) Unmet clinical needs and burden in Angelman syndrome: a review
867 of the literature. Orphanet J Rare Dis 12:164.
868 Williams C, Franco L (2010) Angelman syndrome at the synapse: meeting report of the Angelman
869 Syndrome Foundation's 2009 scientific symposium. J Child Neurol 25:254-261.
870 Williams CA (2005) Neurological aspects of the Angelman syndrome. Brain Dev 27:88-94.
871 Williams CA (2010) The behavioral phenotype of the Angelman syndrome. Am J Med Genet C Semin
872 Med Genet 154C:432-437.

JNeurosci Accepted Manuscript

873 Willuhn I, Tose A, Wanat MJ, Hart AS, Hollon NG, Phillips PE, Schwarting RK, Wöhr M (2014) Phasic
874 dopamine release in the nucleus accumbens in response to pro-social 50 kHz ultrasonic
875 vocalizations in rats. J Neurosci 34:10616-10623.
876 Wöhr M (2021) Measuring mania-like elevated mood through amphetamine-induced 50-kHz ultrasonic
877 vocalizations in rats. Br J Pharmacol 2021:1-19.
878 Wöhr M, Houx B, Schwarting RK, Spruijt B (2008) Effects of experience and context on 50-kHz
879 vocalizations in rats. Physiol Behav 93:766-776.
880 Wöhr M, Schwarting RK (2007) Ultrasonic communication in rats: can playback of 50-kHz calls induce
881 approach behavior? PLoS One 2:e1365.
882 Wöhr M, Schwarting RK (2013) Affective communication in rodents: ultrasonic vocalizations as a tool
883 for research on emotion and motivation. Cell and tissue research 354:81-97.
884 Wöhr M, Seffer D, Schwarting RK (2016) Studying Socio-Affective Communication in Rats through
885 Playback of Ultrasonic Vocalizations. Curr Protoc Neurosci 75:8 35 31-38 35 17.
886 Wöhr M, Kehl M, Borta A, Schanzer A, Schwarting RK, Hoglinger GU (2009) New insights into the
887 relationship of neurogenesis and affect: tickling induces hippocampal cell proliferation in rats
888 emitting appetitive 50-kHz ultrasonic vocalizations. Neuroscience 163:1024-1030.
889 Wolter JM, Mao H, Fragola G, Simon JM, Krantz JL, Bazick HO, Oztemiz B, Stein JL, Zylka MJ (2020)
890 Cas9 gene therapy for Angelman syndrome traps Ube3a-ATS long non-coding RNA. Nature
891 587:281-284.
892 Zucker RS (1989) Short-term synaptic plasticity. Annu Rev Neurosci 12:13-31.
893 Zucker RS, Regehr WG (2002) Short-term synaptic plasticity. Annu Rev Physiol 64:355-405.
894

895 **Data Availability**

896 Data are available from the corresponding author upon request.

JNeurosci Accepted Manuscript

897

898 **Figure Legends**

899

900 **Figure 1.** Overabundant emission of laughter-like 50-kHz calls in juvenile *Ube3a*$^{mat-/pat+}$ rats. **(A)**
901 Example images of the manipulations used to mimic social play and elicit ultrasonic vocalizations (USV).
902 **(B)** Example spectrograms of USV from a wildtype littermate control (*Ube3a*$^{mat+/pat+}$; mat+/pat+; upper)
903 and *Ube3a*$^{mat-/pat+}$ rat (mat-/pat+; lower). **(C)** Across five days of heterospecific play sessions, 50-kHz
904 USV emission increased with repeated testing in both mat-/pat+ (*n*=25) and controls (*n*=25), but the
905 emission rate was substantially elevated in mat-/pat+. **(D)** On average, mat-/pat+ rats produced 50-kHz
906 USV at more than twice the rate of controls. **(E)** Specifically, 50-kHz calling was abnormally high during
907 the break and belly tickle phases, with trending increases during neck tickle, push and drill, and flip over.
908 **(F)** Prior to the onset of play, mat-/pat+ rats emitted anticipatory 50-kHz USV at more than three times
909 the rate of controls. **(G)** Production of short 22-kHz USV was low, did not differ between genotypes, and
910 did not change over subsequent play sessions. **(H)** The rates of 50-kHz and short 22-kHz calling during
911 empty cage exploration were comparable between genotypes (mat+/pat+, *n*=32; mat-/pat+, *n*=29), as were
912 the **(I)** 50-kHz and short 22-kHz calling rates in response to hearing playback of conspecific 50-kHz USV
913 (mat+/pat+, *n*=9; mat-/pat+, *n*=12). Call features did not differ by genotype: **(J)** The average duration and
914 **(K)** peak frequency of spontaneous 50-kHz calls made during exploration of an empty cage was
915 comparable between mat-/pat+ (*n*=23) and mat+/pat+ rats (*n*=25). **(L)** The average duration and **(M)**
916 average peak frequency of short 22-kHz calls made within an empty cage were also similar between
917 genotypes (mat+/pat+, *n*=6; mat-/pat+, *n*=7). **(N)** For 50-kHz USV emitted in response to hearing
918 playback of natural pre-recorded 50-kHz rat USV, average duration and **(O)** average peak frequency were
919 comparable between mat-/pat+ rats (*n*=12) and wildtype littermates (*n*=9). **(P)** There was no genotype
920 effect on the average duration or **(Q)** average peak frequency of short 22-kHz calls made during USV
921 playback (mat+/pat+, *n*=3; mat-/pat+, *n*=2). Of note, long 22-kHz USV known to function as "alarm

JNeurosci Accepted Manuscript

922 calls" were very rarely observed, indicating that our paradigms were not aversive. Data are depicted as
923 mean ± S.E.M. C: **p<0.01, repeated measures ANOVA. D, F: ***p<0.001, **p<0.01, Mann-Whitney
924 test. E: *p<0.05, $^{\#}p$<0.06, repeated measures ANOVA, Holm-Sidak's *post-hoc*.
925
926 **Figure 2.** Intact social interest but deficient expression of key social interaction behaviors in juvenile
927 *Ube3a*$^{mat-/pat+}$ rats. **(A)** During a 10-min interaction session with a novel same-sex wildtype conspecific,
928 *Ube3a*$^{mat-/pat+}$ rats (mat-/pat+; n=12) spent similar amounts of time social sniffing, **(B)** anogenital sniffing,
929 **(C)** self-grooming, and **(D)** exploring the arena compared to wildtype littermate controls (*Ube3a*$^{mat+/pat+}$;
930 mat+/pat+; n=10). **(E)** Robust deficits, however, were discovered in the time spent following or chasing
931 and **(F)** rough-and-tumble playing. **(G)** The number of push pasts were similar across genotypes but **(H)**
932 there was a trend for mat-/pat+ to less frequently push under or crawl over and **(I)** mat-/pat+ rats did not
933 perform nearly as many pounces as wildtype littermates. **(J)** A separate test of olfactory discrimination
934 revealed normal sniff times of social and non-social scents. Time spent investigating novel odors was
935 similar for mat-/pat+ (n=7) and mat+/pat+ rats (n=7) and both groups spent more time investigating a
936 social scent compared to a non-social vanilla odor. Data are depicted as mean ± S.E.M. E-I: **p<0.01,
937 *p<0.05, $^{\#}p$<0.065, Mann-Whitney test. J: *p<0.05, repeated measures ANOVA, Holm-Sidak's *post-hoc*.
938
939 **Figure 3.** Abnormal gait in *Ube3a*$^{mat-/pat+}$ rats. **(A)** While treadmill walking, *Ube3a*$^{mat-/pat+}$ rats (mat-/pat+;
940 n=23) displayed aberrant propulsion time (time from maximal paw contact with belt to just before liftoff)
941 in both sets of limbs. Compared to wildtype littermates (*Ube3a*$^{mat+/pat+}$; mat+/pat+; n=23), propulsion time
942 was decreased in the forelimbs and increased in hindlimbs. **(B)** Brake time (time from initial to maximal
943 paw contact with belt) was significantly elevated in the forelimbs of mat-/pat+ while a trending reduction
944 in hindlimb brake time was found (p=0.150). **(C)** Swing time (no paw contact with the belt) and **(D)** stride
945 time (sum of swing and stance time) were similar across genotypes. **(E)** Example paw prints illustrating
946 the spatial gait parameters depicted in panels F, G, and H. **(F)** Stride length did not differ between groups,
947 but **(G)** forelimb stance width was narrower and **(H)** absolute paw angle for the forelimbs was greater,

JNeurosci Accepted Manuscript

948 indicating more external rotation in mat-/pat+ rats. **(I)** No significant difference in gait symmetry (ratio of
949 forelimb to hindlimb stepping frequency) was detected. Data are depicted as mean ± S.E.M. **p<0.01,
950 *p<0.05, repeated measures ANOVA, Holm-Sidak's *post-hoc*.
951
952 **Figure 4.** Impaired learning and memory in *Ube3a*$^{mat-/pat+}$ rats. **(A)** During fear conditioning training,
953 juvenile *Ube3a*$^{mat-/pat+}$ (mat-/pat+; n=12) and wildtype littermate controls (*Ube3a*$^{mat+/pat+}$; mat+/pat+; n=20)
954 showed similar increases in freezing post-training. **(B)** When returned to the training context 24 hrs
955 following training, mat-/pat+ rats exhibited a similar level of freezing to wildtypes. **(C)** When introduced
956 to a novel context 48 hrs after training, no difference in freezing pre-cue was found but mat-/pat+ rats
957 froze for less than half the time of wildtypes during presentation of the auditory cue. A separate
958 sensorimotor test confirmed intact auditory sensitivity: **(D)** Baseline activity within the testing apparatus
959 was comparable between mat-/pat+ (n=10) and mat+/pat+ rats (n=14). **(E)** There was no effect of
960 genotype on the startle response to a 120 decibel (dB) startle stimulus. **(F)** Prepulse inhibition of the
961 startle response was generally reduced in adult mat-/pat+ rats. **(G)** Spontaneous arm alternation during Y-
962 maze exploration was significantly reduced in adult mat-/pat+ rats (n=24) compared to wildtype
963 littermates (n=24). **(H)** Mat-/pat+ rats made 40% more errors and **(I)** made more entries into the maze
964 arms. Bars indicate mean ± S.E.M. A, C: ****p<0.0001, ***p<0.001, repeated measures ANOVA,
965 Holm-Sidak's *post-hoc*. F: *p<0.05, repeated measures ANOVA main effect. G-I: ***p<0.001, **p<0.01,
966 Student's *t*-test.
967
968 **Figure 5.** Reduced hippocampal long-term potentiation (LTP) in *Ube3a*$^{mat-/pat+}$ rats. **(A)** Normal basal
969 synaptic transmission as measured by presynaptic fiber volley amplitudes and postsynaptic fEPSP slopes
970 for responses elicited by different intensities of SC fiber stimulation in *Ube3a*$^{mat-/pat+}$ (mat-/pat+; n=16)
971 and wildtype littermate (*Ube3a*$^{mat+/pat+}$; mat+/pat+; n=11) hippocampal slices. **(B)** Paired-pulse facilitation
972 was unchanged at mat-/pat+ SC-CA1 synapses compared to mat+/pat+ (n=15 mat+/pat+ and n=20 mat-
973 /pat+ slices). (Right) Traces represent fEPSPs evoked by stimulation pulses delivered with a 50 msec

JNeurosci Accepted Manuscript

974 interpulse interval. Scale bars: 0.5 mV, 25 msec. **(C)** High frequency stimulation (HFS)-induced LTP in
975 mat+/pat+ (*n*=11) was significantly greater compared to mat-/pat+ (*n*=16). Traces at right represent
976 superimposed fEPSPs recorded during baseline and 60 min after HFS. Scale bars: 1 mV, 5 msec. **(D)**
977 Summary graph of average percentage potentiation relative to baseline demonstrating that mat+/pat+
978 exhibited significantly enhanced SC-CA1 LTP at 60 min after HFS (delivered at time = 0), fEPSPs were
979 potentiated to 160 ± 7% of baseline in mat+/pat+ (*n*=11) and were 127 ± 5% of baseline in mat-/pat+
980 slices (*n*=16). Data were collected from two rats per genotype. ****p<0.0001, Student's *t*-test.
981
982 **Figure 6.** Neuroanatomical pathology in *Ube3a*$^{mat-/pat+}$ rats revealed by high-resolution magnetic
983 resonance imaging (MRI). (Left) Slice series comparing absolute volume (mm^3) of juvenile and adult
984 populations of *Ube3a*$^{mat-/pat+}$ (mat-/pat+) rats and wildtype littermates (*Ube3a*$^{mat+/pat+}$; mat+/pat+). Red to
985 yellow coloration indicates increased volume compared to wildtype whereas dark blue to light blue
986 indicates decreased volume. The leftmost column is data on juvenile mat-/pat+ rats from Berg et al.
987 (2020) and the center column illustrates the same slices on the adult dataset presented here. Most notably,
988 total brain volume was 6.0% smaller in mat-/pat+ rats compared to wildtype. Additionally, the third
989 column shows the genotype by age interaction highlighting several regions of interest, (right) four of
990 which are shown in panels A-D. Namely, **(A)** fiber tracts, **(B)** the hypothalamus, **(C)** the hippocampal
991 region, and **(D)** the thalamus. Full detail of regional findings for adult animals and the interaction effect
992 are described in Figures 6-1 and 6-2. Group sizes: juvenile mat+/pat, *n*=29; juvenile mat-/pat+, *n*=25;
993 adult mat+/pat+, *n*=23; adult mat-/pat+, *n*=24. Bars indicate mean ± S.E.M. ****p<0.0001, **p<0.01,
994 two-way ANOVA, Holm-Sidak's *post-hoc*.
995

996 **Extended Data Figure Legends**

997

998 **Figure 6-1.** Brain volumes for adult *Ube3a*$^{mat-/pat+}$ rats and wildtype littermates.
999

JNeurosci Accepted Manuscript

1000 **Figure 6-2.** Age by genotype interaction for absolute brain volumes of juvenile and adult *Ube3a*$^{mat-/pat+}$

1001 rats and wildtype littermates.

JNeurosci Accepted Manuscript

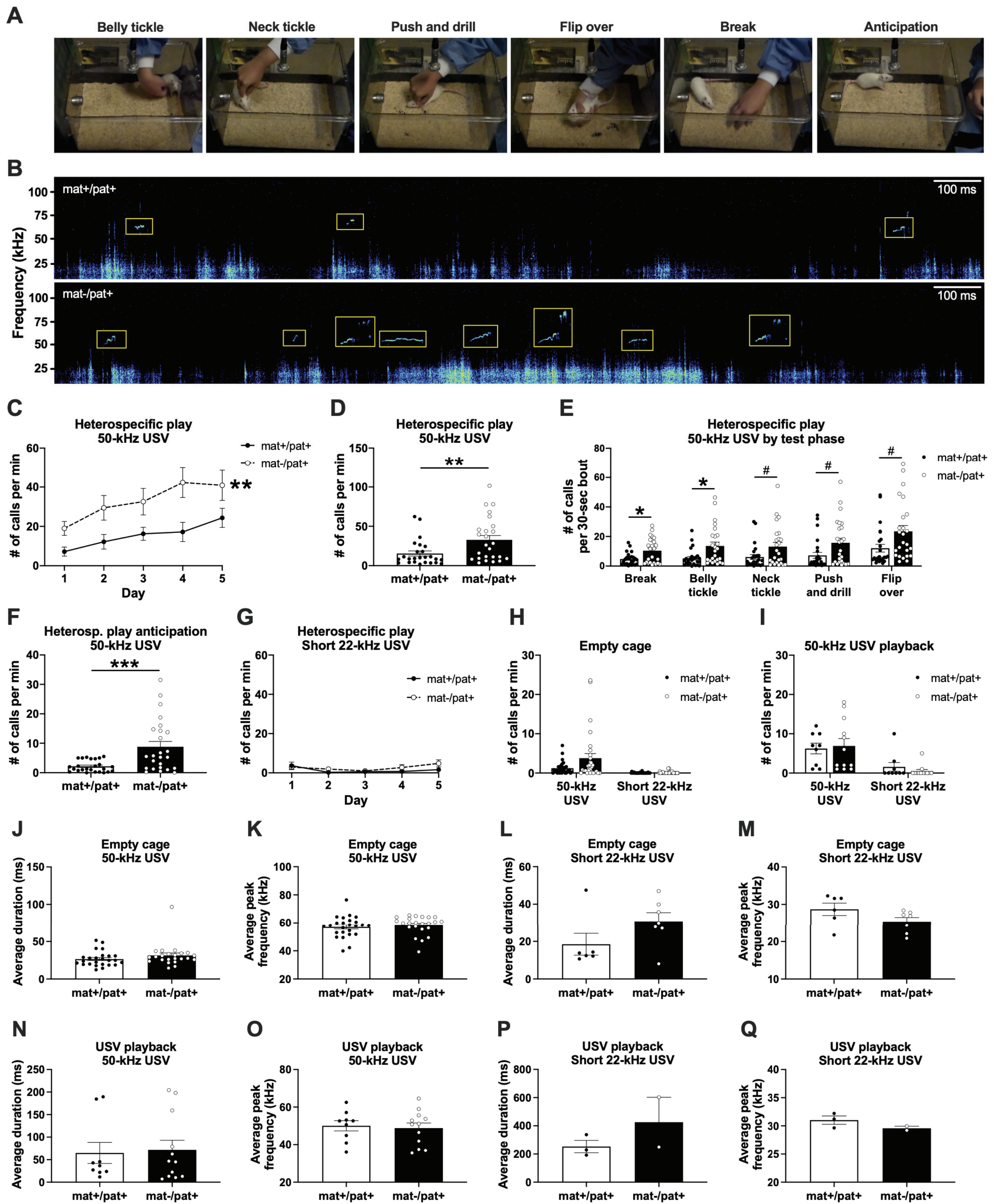

JNeurosci Accepted Manuscript

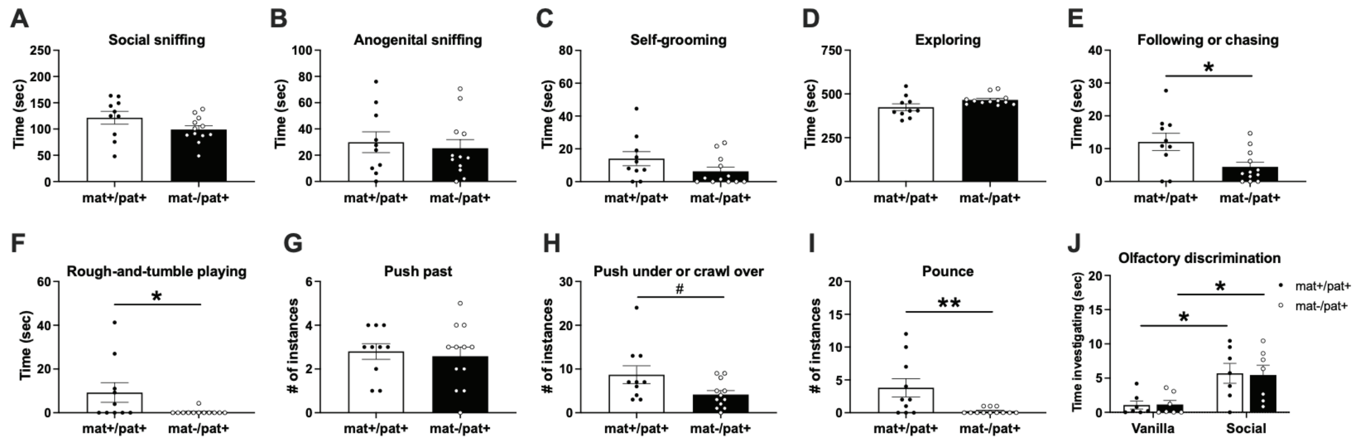

JNeurosci Accepted Manuscript

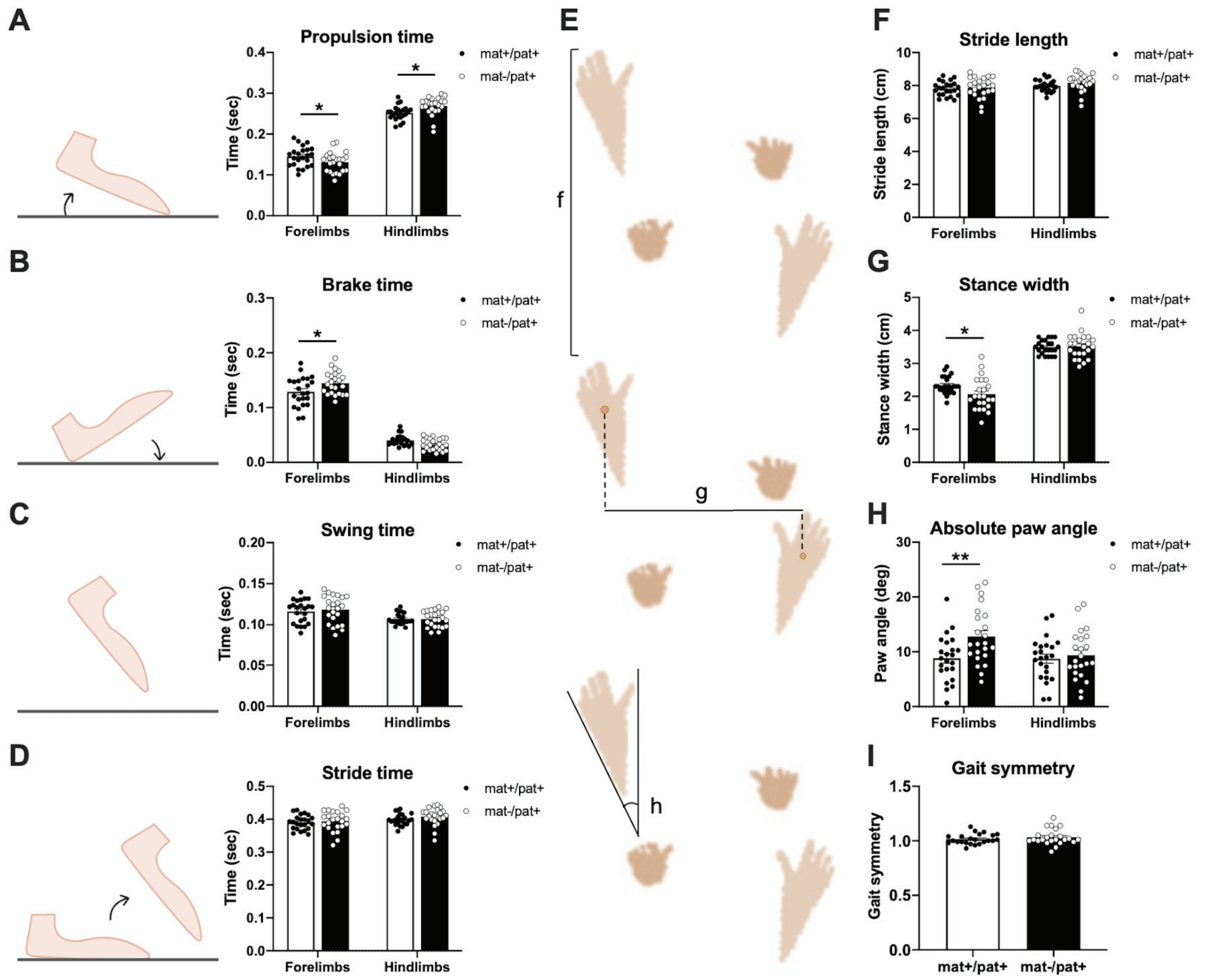

JNeurosci Accepted Manuscript

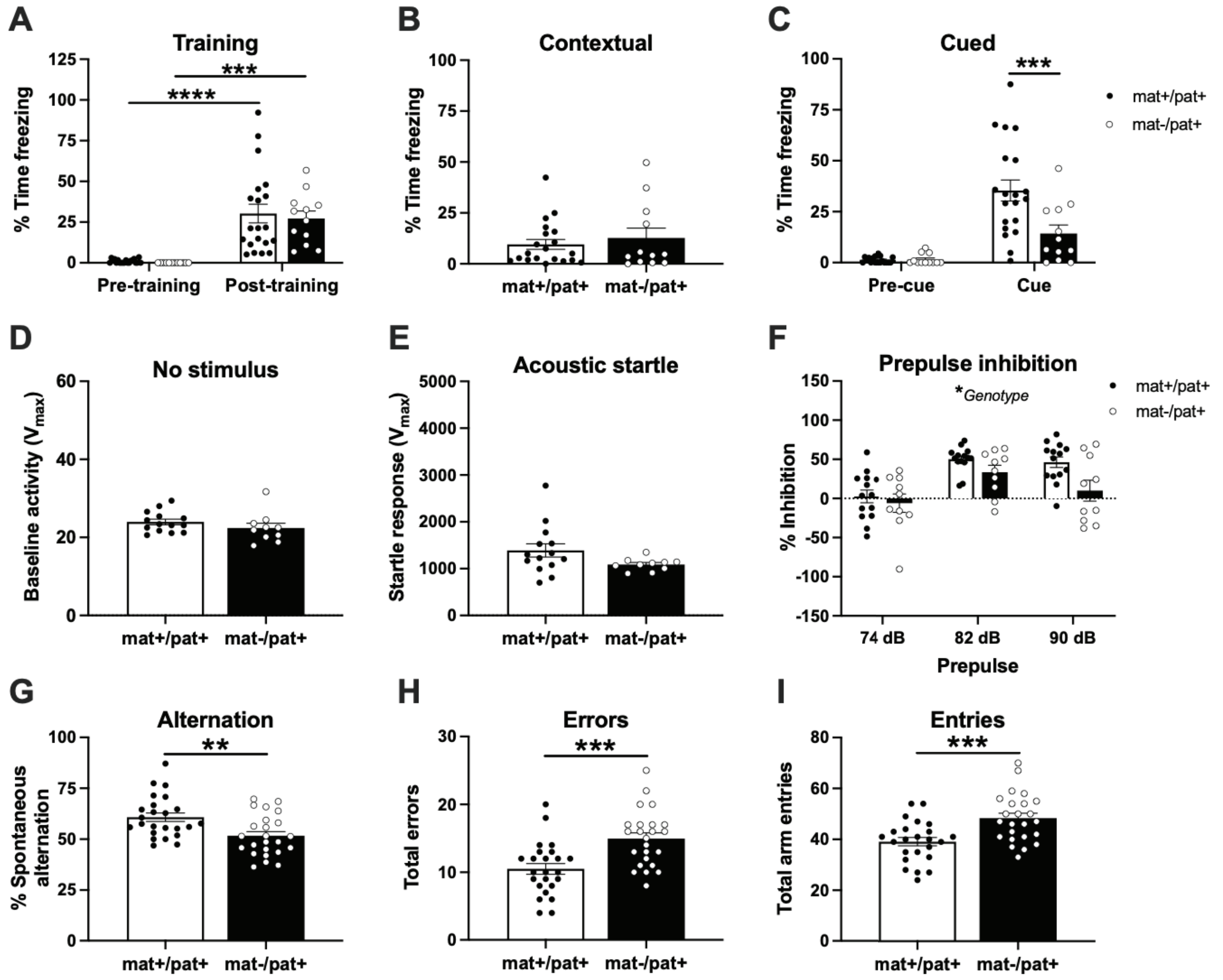

JNeurosci Accepted Manuscript

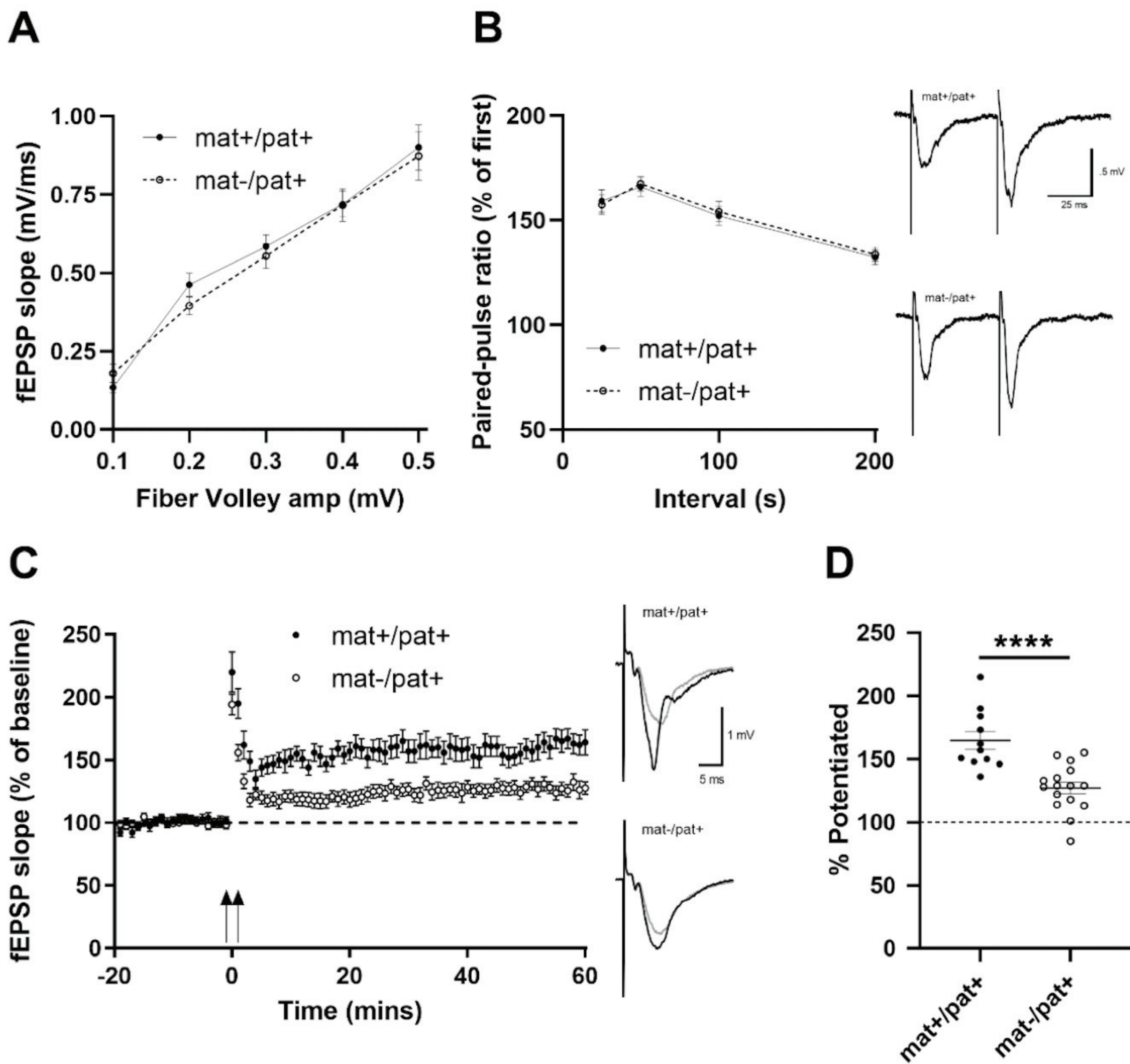

JNeurosci Accepted Manuscript